Applied Thermal Engineering

Experimental and numerical analysis of the melting evolution in phase change materials embedded with aluminum foams with different morphologies and orientations

--Manuscript Draft--

Manuscript Number:	
Article Type:	Original Research Papers
Keywords:	Thermal energy storage, Phase Change Materials, Metal foams, Experimental and numerical analysis, Melting front, Local thermal non-equilibrium
Corresponding Author:	Mauro Mameli ITALY
First Author:	Marcello Iasiello, PhD
Order of Authors:	Marcello Iasiello, PhD
	Mauro Mameli
	Sauro Filippeschi
	Nicola Bianco, PhD
Abstract:	Phase Change Materials (PCM) are promising materials for thermal energy storage systems. Since they present a relatively low thermal conductivity, they are often embedded in an open cell a metallic foam to enhance the overall thermal conductivity. In this paper, both experimental and numerical results on PCMs coupled with aluminum foams under different heat fluxes, porosities, number of Pores Per Inch (PPIs) and orientation are presented. The test cell is equipped with a Zincum Selenide window that allows to capture the whole temperature distribution by means of a IR camera. The melting front position in time is tracked by means of a MATLAB® algorithm based on IR camera images that are useful for a more robust tracking of melting front. Numerical simulations are performed with references to the porous media volume-averaged approach, under the assumption of local thermal non-equilibrium between the two phases. The most updated correlations for the porous media closing coefficients are taken from the literature. All the experiments are compared with numerical simulations, showing a very good agreement. After showing the effects of the different input parameters on melting front evolution, an analysis in terms of different convective heat losses to the environment and melting temperature range is presented to appreciate how these two variables affect the melting front position. Finally, total melting front evolution has been compared between experiments and simulations, showing a good agreement. This has been evaluated for different conditions, showing that a decrease in the porosity drastically reduces the melting time, while PPI has no relevant effect and small effects can be observed from orientation.
Suggested Reviewers:	Simone Mancin, PhD Lecturer, University of Padova: Universita degli Studi di Padova simone.mancin@unipd.it
	Giuseppe Zummo, PhD ENEA Centro Ricerche Casaccia giuseppe.zummo@enea.it
	Khalid Lafdi, PhD info@udayton.edu

DESTEC

UNIVERSITÀ DI PISA

Dipartimento di Ingegneria dell'Energia, dei Sistemi, del Territorio e delle Costruzioni

Largo Lucio Lazzarino – 56122, Pisa (Italy)
Tel. +39 050 2217300, Fax + 39 050 2217333
Partita IVA 00286820501 VAT No. IT00286820501
Codice fiscale 80003670504

To,
Prof. Dr. C.N. Markides
Editor-in-Chief
Applied Thermal Engineering
Imperial College London, London, UK

Mauro Mameli
University of Pisa, DESTEC
Thermal Physics Laboratory
Tel: +39 050 2217166
E-mail: mauro.mameli@unipi.it

Date: September 4th, 2020

Dear Prof. Markides,

Please find in attachment the manuscript entitled

Experimental and numerical analysis of the melting evolution in phase change materials embedded with aluminum foams with different morphologies and orientations

Authors: Marcello Iasiello, Mauro Mameli, Sauro Filippeschi and Nicola Bianco

This is the result of a very fruitful collaboration between the University of Pisa and the University of Naples (Federico II) where the first dealt mainly with the experimental investigations and the second with the numerical modeling and validation.

Passive thermal storage/management employing Phase Change Materials is gaining more and more interest in the scientific community due to the very wide number of applications. For this reason, the authors believe that the Applied thermal Engineering is the most suitable journal for disseminating such information to the scientific community and they really appreciate if you could consider the attached manuscript for publication.

With best regards,
yours sincerely

Mauro Mameli
(Corresponding Author)

Experimental and numerical analysis of the melting evolution in phase change materials embedded with aluminum foams with different morphologies and orientations

Marcello Iasiello[*], Mauro Mameli[,#], Sauro Filippeschi[**] and Nicola Bianco[*]**

[*] Dipartimento di Ingegneria Industriale - Università degli Studi di Napoli Federico II - Piazzale Tecchio, 80 - 80125 – Napoli – Italy

[**] Dipartimento dell'Energia dei Sistemi del Territorio e delle Costruzioni - Università di Pisa – Largo Lazzarino, 2 - 56121 – Pisa – Italy

[#]corresponding author: mauro.mameli@unipi.it

HIGHLIGHTS

- Experimental and numerical results on heat transfer in PCM/foam are presented.
- Morphology, orientation effects, and IR-camera melting front tracking, are shown.
- Melting front and fraction comparisons show a good agreement for all cases.
- Liquid phase velocities are shown to appreciate morphology and orientation effects.
- Porosity has a higher impact on melting compared to PPI and orientation.

Experimental and numerical analysis of the melting evolution in phase change materials embedded with aluminum foams with different morphologies and orientations

Marcello Iasiello[*], Mauro Mameli[,#], Sauro Filippeschi[**] and Nicola Bianco[*]**

[*] Dipartimento di Ingegneria Industriale - Università degli Studi di Napoli Federico II - Piazzale Tecchio, 80 - 80125 – Napoli – Italy

[**] Dipartimento dell'Energia dei Sistemi del Territorio e delle Costruzioni - Università di Pisa – Largo Lazzarino, 2 - 56121 – Pisa – Italy

[#]corresponding author: mauro.mameli@unipi.it

Abstract

Phase Change Materials (PCM) are promising materials for thermal energy storage systems. Since they present a relatively low thermal conductivity, they are often embedded in an open cell a metallic foam to enhance the overall thermal conductivity. In this paper, both experimental and numerical results on PCMs coupled with aluminum foams under different heat fluxes, porosities, number of Pores Per Inch (PPIs) and orientation are presented. The test cell is equipped with a Zincum Selenide window that allows to capture the whole temperature distribution by means of a IR camera. The melting front position in time is tracked by means of a MATLAB® algorithm based on IR camera images that are useful for a more robust tracking of melting front. Numerical simulations are performed with references to the porous media volume-averaged approach, under the assumption of local thermal non-equilibrium between the two phases. The most updated correlations for the porous media closing coefficients are taken from the literature. All the experiments are compared with numerical simulations, showing a very good agreement. After showing the effects of the different input parameters on melting front evolution, an analysis in terms of different convective heat losses to the environment and melting temperature range is presented to appreciate how these two variables affect the melting front position. Finally, total melting front evolution has been compared between experiments and simulations, showing a good agreement. This has been evaluated for different conditions, showing that a decrease in the porosity drastically reduces the melting time, while PPI has no relevant effect and small effects can be observed from orientation.

Keywords

Thermal energy storage, Phase Change Materials, Metal foams, Experimental and numerical analysis, Melting front, Local thermal non-equilibrium.

Nomenclature

Latin symbols

A_{mush}	volume force constant (kg/m^3 s)
b_{mush}	volume force constant
C	specific heat capacity (J/kg K)
d_c	cell size (m)
d_s	strut size (m)
$\mathbf{g}$	gravity acceleration (m/s^2)
G	geometric function
h	heat transfer coefficient (W/m^2 K)
h_c	interfacial heat transfer coefficient (W/m^2 K)
h_v	volumetric heat transfer coefficient (W/m^3 K)
k	thermal conductivity (W/m K)
K	permeability (m^2)
L	length (m)
Nu_s	strut Nusselt number
p	pressure (Pa)
q	heat flux modulus (W/m^2)
Ra_s^*	strut Rayleigh number
S	volume force term (kg/m^3 s)
S_v	specific surface area (1/m)
t	time (s)
T	temperature (K)
$\mathbf{u}$	velocity vector (m/s)
x, y	Cartesian coordinates (m)

Greek symbols

α	isobaric compressibility (1/K)
β	melting fraction function
ε	porosity
λ	latent heat of fusion (J/kg K)
μ	viscosity (Pa s)
ρ	density (kg/m^3)

Subscripts

d	dispersion
eff	effective
in	incoming
m	melting
PCM	phase Change Material
$Pelt$	Peltier

1. Introduction

Phase change materials are widely known to be a promising class of materials for thermal energy storage [1]. Indeed, they present the ability of storing high amounts of energy under low temperature variations under a customized melting temperature. One of the shortcomings about PCMs is their low thermal conductivity. Many techniques like nanoparticles, wire meshes of microencapsulation [2] have been proposed to overcome this issue. Another option is to employ a net-like structure made up of several connected metallic ligaments in which various cells separated by pores can be distinguished, also known as metallic foam [3]. Because of the metal high thermal conductivity, the overall thermal conductivity of the PCM/foam can be strongly enhanced [4].

Various solutions for thermal energy storage based on PCM/foams have been proposed through the years. These solutions were focused mainly on aspects like which are the best foam morphological characteristics to enhance heat transfer and reduce surface temperatures and melting time. An annulus of two concentric cylinders with PCM and high thermal conductivity foam has been numerically analyzed by Mesalhy et al. [5], showing that especially low porosity foams can enhance heat transfer and melting rate, even if they also dump convection motions. Experiments on different porosity and PPI aluminum foams with PCMs have been carried out by Lafdi et al. [6], showing that lower porosity cause lower heater temperatures, while higher porosity and lower PPIs make steady-state condition to be reached in a shorter time because of the higher convection effect. A RT58 phase change material with metal foams heated from below have been analyzed by Zhao et al. [7], showing that thermal performances are enhanced by natural convection and overall heat transfer rates can be enhanced of 3-10 times depending on metallic foam employed. Tian and Zhao [8] numerically showed that PCMs heated from below have improved characteristics especially with lower porosities and higher pore densities, even if natural convection is suppressed because of metal foam large flow resistance. Experimental and numerical studies of a copper foam filled with paraffin in a vertical orientation and heated from a vertical plate have been shown by Li et al. [9]. The authors found a very good agreement between experiments and predictions, and they show that more uniform temperatures can be achieved with lower porosity to improve conduction or with lower pore density to enhance natural convection. Besides, they also found that lower porosities make solid/liquid interface movement to be faster. Xiao et al. [10] experimentally analyzed open-cell metal foams coupled with pure paraffin, showing that thermal conductivity were drastically enhanced of about between thirteen and fourty-four times than that of pure paraffin, with the former referred to 96.95% porosity and the latter referred to 88.89% porosity. Experiments of copper foams with different PPIs coupled with PCMs heated from below have been performed by Mancin et al. [11]. The authors concluded that foam matrix improves heat transfer capabilities of the system because of lower surface temperatures achieved, while PPI effects have not been found to be relevant. Yang et al. [12] performed analytical, numerical and experimental studies of fluid saturated solidification in metal foams, concluding that full solidification time can be reduced of three times when a foam is placed in water, especially with non-hollow ligaments. The authors report that this solution could be economically convenient because of boundary wall temperature reduction and coefficient of performance enhancement. Microencapsulated phase change materials in metal foams have been experimentally analyzed by Li et al. [13] by varying angles to appreciate natural convection effects. Authors concluded that metal foam can reduce surface temperature of about 47%, with lower porosity configuration as the best in terms of thermal performances. Di Giorgio et al. [14] numerically analyzed aluminum foams with phase change materials, including also a new methodology to compute interfacial heat transfer between foam and PCM An empirical correlation based on experiments performed on PCMs with foams with different PPIs, applied heat fluxes and PCM melting temperatures has been proposed by Diani and Campanale [15]. They showed that dimensionless temperature is correlated with Fourier number multiplied with Stefan number by means of a power law, with small deviations from experiments. Pore-scale analysis by employing a body centered cubic geometrical model have been performed by Ferfera et al. [16], showing that lower porosity causes higher thermal conductivity and smaller pore diameters uniform melting front and temperature inside the composite. Comprehensive

critical reviews on the argument can be also found in [17, 18]. Tauseef-ur-Rehman et al. [17] reviewed influences of metallic foam matrixes on PCMs to appreciate thermal conductivity augmentation. From their review, they underline that porous materials/foam can enhance heat transfer/thermal conductivity of 3-500 times, and that an effort to analyze aspects like exergy efficiency, the effects of graphene coating or very low melting temperature PCMs, is needed. Zhang et al. [18] reviewed both experimental and numerical studies on porous shape stabilized PCMs, with an emphasis on metallic foams as the porous material. They underlined that there is a lack of results about middle-high melting temperature PCMs coupled with foams, nano porous materials coupled with PCMs and appropriate investigation of pore-scale phenomena, especially with references to mesoporous, microporous and hierarchical porous materials.

From the state-of-art just described, even if many results about PCM coupled with foams and related advantages have been presented in literature, many aspects have not been properly covered yet. Most of the works assume a vertical configuration for the domain, thus heat flux is orthogonal to the gravity direction. Very few papers, both numerical and experimental, have been proposed about the effects of natural convection when device orientation changes. This aspect is very important since natural convection can have an important role because of liquid PCM movement, and this is influenced by orientation or gravity vector intensity. Filippeschi et al. [19] experimentally analyzed the role of convection in a melting composite material consisting in a paraffin wax and aluminum foams with different morphologies tested in a hypergravity environment. The experiments show that the hypergravity condition accelerates the melting process: it is 12% faster ranging from 5 g to 10 g. A natural convection regime was observed in all of the experiments and it accelerates the melting process. A critical analysis of the scaling criterion in the literature has been qualitatively done and a modified Rayleigh number is proposed to characterize the melting process. Very recently, Hu et al. [17] numerically analyzed phase change materials saturated in metal foams to analyze heating and contact conditions. In particular, they investigated top, left and bottom heating, and different contact gaps. Simulations are performed based on volume-averaged technique, and the authors conclude that heating condition can affect phase change and thermal charging. The Contact between the foam struts and heated wall has been found to not have a relevant effect under top heating, while in left heating it can affect melting time. Another relevant effect that have not been properly analyzed is the method used to establish melting front position from experiments. In many studies, this have been extrapolated from standard camera recording, as for example done in [13, 18]. However, with this method one can just roughly establish where melting front is by observing that solid and liquid paraffin present different colors. Besides, this method could be unreliable when paraffin is coupled with a foam, because of the presence of metallic struts that makes confusion when melting front needs to be evaluated with a rigorous technique. Infrared camera has been used by Zhang et al. [18] to validate their model in terms of temperature fields, which is better for validation of numerical models, without any mention about melting front, that has been evaluated with conventional camera. Chen et al. [19] also employed IR camera in their experiments to establish temperatures inside PCM and foam, and from their results one can think about evaluating melting front from these measurements, even if they perform this analysis from conventional camera. Filippeschi et al. [19] coupled a visible and IR inspections to observe the melting process evolution over time and to evaluate melting front location. They used IR images to quantitively detect the dynamic evolution of the melting front with a good accuracy (<2 % on the melting area).

Based on the literature survey, one can conclude that orientation effects have not been already properly investigated in such devices. Besides, an appropriate and robust method to establish melting front position is mandatory to simulate charge/discharge period, which gives the amount of energy stored/released in the PCM/foam device. In this contribution, both experimental and numerical results for paraffin coupled with aluminum foams are presented for different porosity and PPI aluminum foams, with either vertical or horizontal orientations, for a total of 12 cases. The objective here is to analyze morphology and orientation effects, and to provide a robust method to establish melting front based on IR images based on both experimental and numerical approaches. Experiments have been performed under a uniform heat flux boundary condition provided by a Peltier cell. After monitoring temperature evolution with

an IR camera, melting front position is evaluated from such measurements by employing MATLAB in-house algorithm. Numerical model is built up with references to the local thermal non-equilibrium porous media model. After comprehensive comparisons between melting front evaluated with the new technique and numerical simulations, simulations of other effects like orientation, phase change temperature range and convective losses will be presented.

2. Mathematical model

The investigated PCM is a paraffin (Ph EUR, BP, NF CAS 8002-74-2) while metal foams herein investigated are aluminum foam manufactured by ERG Aerospace. PCM thermophysical properties are resumed in Table 1 while investigated foams present between 0.88 and 0.95 porosities and 10 to 40 PPIs. Details of the experiments will be shown later. The experimental setup of the PCM/foam is described in detail in the experiments section afterwards, together with foams investigated. Because it is assumed that all the walls of the PCM/foam are adiabatic except the one that faces Peltier cell, the geometrical model for the prediction is a 2D square with a side L = 0.05 m, where the heat flux is orthogonal to the gravity vector (vertical orientation) or parallel (horizontal orientation). The computational investigated domain is shown in Fig. 1.

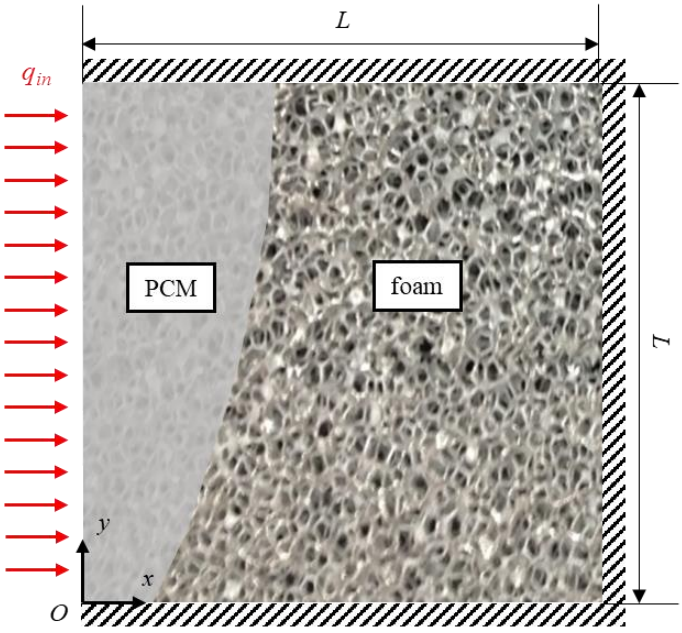

Fig 1 – Computational domain

Governing equations are written with references to porous media theory [23] and by assuming local thermal non-equilibrium between the two phases [24]. For each Representative Elementary Volume (REV) of the two components (PCM and aluminum foam), mass, momentum and energy equations are written under the assumptions of incompressible laminar flow, Boussinesq assumption and negligible microinertial effects.

$$\frac{\partial \rho_{PCM}}{\partial t} + \nabla \cdot \left(\rho_{PCM} \mathbf{u} \right) = 0 \tag{1}$$

$$\frac{\rho_{PCM}}{\varepsilon\beta} \left(\frac{\partial \mathbf{u}}{\partial t} + \frac{\mathbf{u}}{\varepsilon\beta} \cdot \nabla \mathbf{u} \right) = -\nabla p + \frac{\mu_{PCM}}{\varepsilon\beta} \nabla^2 \mathbf{u} - \frac{\mu_{PCM}}{K} \mathbf{u} + \rho_{PCM} \mathbf{g} \alpha \left[T_{PCM} - \left(T_m - \Delta T_m \right) \right] \beta - S\mathbf{u} \tag{2}$$

$$(\rho C)_{PCM}\left(\varepsilon\frac{\partial T_{PCM}}{\partial t}+\mathbf{u}\cdot\nabla T_{PCM}\right)=\nabla\cdot\left(k_{eff,PCM}\nabla T_{PCM}\right)+h_v\left(T_{foam}-T_{PCM}\right)-\varepsilon\rho_{PCM}\lambda\frac{\partial\beta}{\partial t} \quad (3)$$

$$(1-\varepsilon)(\rho C)_{foam}\frac{\partial T_{foam}}{\partial t}=\nabla\cdot\left(k_{eff,foam}\nabla T_{foam}\right)-h_v\left(T_{foam}-T_{PCM}\right) \quad (4)$$

In the momentum equation, the source term is employed in order to force solution to zero when PCM becomes solid by means of the following term

$$\beta=\begin{cases}10^{-6} & T_{PCM}\le T_m-\Delta T_m\\ \dfrac{T_{PCM}-(T_m-\Delta T_m)}{2\Delta T_m} & T_m-\Delta T_m<T_{PCM}<T_m+\Delta T_m\\ 1 & T_{PCM}\ge T_m+\Delta T_m\end{cases} \quad (5)$$

$$S=A_{mush}\frac{(1-\beta)^2}{b_{mush}+\beta^3} \quad (6)$$

The value 10^{-6} allows to avoid division by zero in the momentum equation (Eq. 2). The function β takes into account melting in the ΔT_m range, and it is smoothed in $T_m \pm \Delta T_m$ in order to make second derivative continuous everywhere. The function Eq. (6) is obtained from Carman-Kozeny equation, thus the mushy zone is modeled as a solid/liquid porous medium. In such equation, A_{mush} is a geometrical constant taken equal to 10^4 while b_{mush} is equal to 10^{-3} to avoid division by zero. Negligible effects of results with higher A_{mush} have been found in Kheirabadi and Groulx [25]. With references to the buoyancy term reported in Eq. 2, this term is multiplied with the function β shown in Eq. (5) in order to help numerical convergence, and also to make buoyancy significant only after melting temperature, with interpolated values in the mushy-zone in order to take into account the simultaneous existence of both phases.

To close the governing equations, the porous media coefficients are required. A resume of correlations here employed is reported in Table 2. Permeability functions are taken from Calmidi [26], while a function that allows to pass from PPIs to cell size is taken from Andreozzi et al. [27]. For the volumetric heat transfer coefficient, a correlation for the Nusselt number is required. Foam struts can be assumed to be cylinders with a diameter equal to the strut diameter d_s, then the correlation valid for cylinders from Churchill and Chu [28] is here employed to obtain interfacial heat transfer coefficient. It is important to remark that this volumetric heat transfer coefficient can be also defined to couple foam with PCM even if it is in the solid phase, and here we assume that the volumetric heat transfer coefficient is independent from the phase. A study on this has been performed by Di Giorgio et al. [14], where coupling coefficients have been derived between solid PCM and foam. Values achieved have been shown to be not so different from volumetric heat transfer coefficients referred to convection when PCM is in the liquid phase. For the PCM effective thermal conductivity, stagnant thermal conductivity is considered with a parallel model (εk_f), while thermal dispersion is considered and modeled with the gradient-diffusion assumption with the correlation from [29]. Finally, foam effective thermal conductivity expression is taken from Iasiello et al. [30] under the assumption of isotropic thermal conduction in foam struts.

For the boundary conditions, it is assumed that all the walls present a velocity equal to zero. For the energy equations, except for the exposed surface we assume adiabatic surfaces everywhere, thus external convection losses are neglected. Heat flux comes in from the left side of the domain and this is modeled with a second-kind boundary condition. By neglecting thermal dispersions between Peltier cell and PCM/foam box, it is here assumed that heat flux is split in the two phases (PCM and foam) in parallel, thus weighted based on porosity.

$$q_{PCM} = \varepsilon q_{in} = -k_{eff,PCM} \left. \frac{\partial T_{PCM}}{\partial y} \right|_{x=0} \tag{7a}$$

$$q_{foam} = (1-\varepsilon) q_{in} = -k_{eff,foam} \left. \frac{\partial T_{foam}}{\partial y} \right|_{x=0} \tag{7b}$$

This assumption is reliable since effective thermal conductivities of the two phases are more or less of the same order of magnitude, thus one can assume that heat flux can be split based on porosity based on boundary condition scaling from Hwang et al. [31].

Table 1 – PCM and foam thermophysical properties

Property	PCM	Foam
Density (ρ, kg/m3)	850	2700
Thermal conductivity (k, W/m K)	0.15 (liquid) 0.20 (solid)	220
Specific heat capacity (C, J/kg K)	2490	900
Viscosity (μ, Pa s)	$3.85 \cdot 10^{-3}$	
Thermal expansion coefficient (α, 1/K)	$7.78 \cdot 10^{-4}$	
Latent heat of fusion (λ, kJ/kg)	185	
Melting temperature (T_m, °C)	57	
Melting range (ΔT_m, °C)	1	

Table 2 – Closing coefficients for Eqs. (1-6)

Coefficient	Espression	Reference
Permeability (K, m^2)	$K = 0.00073(1-\varepsilon)^{-0.224}\left(\frac{d_s}{d_c}\right)^{-1.11}$	[26]
	$\frac{d_s}{d_c} = \frac{1.18}{G}\sqrt{\frac{1-\varepsilon}{3\pi}}$	
	$G = 1 - e^{\left[-(1-\varepsilon)/0.04\right]}$	
	$d_c = \left[-0.921\ln(PPI) + 5.3564\right]10^{-3}$	[27]
Volumetric heat transfer coefficient (h_v, W/m^3 K)	$h_v = h_c S_v = \mathrm{Nu}_s \frac{k_{PCM}}{d_s} S_v$	[26]
	$S_v = \frac{G}{0.59}\frac{3\pi d_s}{d_c^2}$	
	$\mathrm{Ra}_s^* = \left(\rho^2 C\right)_{PCM} \alpha \mathbf{g} q_{in} d_s^4 \Big/ \left(k^2 \mu\right)_{PCM}$	
	$\mathrm{Nu}_s = 0.36 + 0.521\left\{\frac{\mathrm{Ra}_s^*}{\left[1+\left(0.442/\mathrm{Pr}\right)^{9/16}\right]^{16/9}}\right\}^{1/4}$	[28]
PCM effective thermal conductivity ($k_{eff,PCM}$, W/m K)	$k_{eff,PCM} = \varepsilon k_{PCM} + k_d$	[29]
	$k_d = \frac{0.36}{1-\varepsilon}\left(\rho C\right)_{PCM} d_s \lvert\mathbf{u}\rvert$	
Foam effective thermal conductivity ($k_{eff,foam}$, W/m K)	$k_{eff,s} = 0.316(1-\varepsilon)k_{foam}$	[30]

Finally, governing equations with the appropriate closing coefficients and boundary conditions are solved with a finite element commercial code COMSOL Multiphysics. A mapped quadratic grid of 100x100 elements has been used, where this value has been checked on temperatures achieved during transient simulations with higher number of elements. Negligible differences have been found, thus 100x100 elements were sufficiently enough. Time-dependent problem is solved with a free-time step algorithm. The PARDISO linear solver is used with a convergence criterion of 10^{-3} for each investigated time step. Time step convergence has been checked, and a maximum time step of Δt = 0.1 s has been used here for time simulations.

3. Experimental setup

Experimental apparatus has been already described in previous papers [19] and it is here briefly resumed. A scheme of the experimental test cell made up by heating/cooling system, bounding box and composite material is presented in Fig. 2. It consists of the heating/cooling system, the composite material, and the containing box. The heating system is made of a Peltier module (40x40x5 mm) with two sides respectively connected with an aluminum plate on which the foam is brazed, and with an active cooling system by means of a high thermal conductive paste.

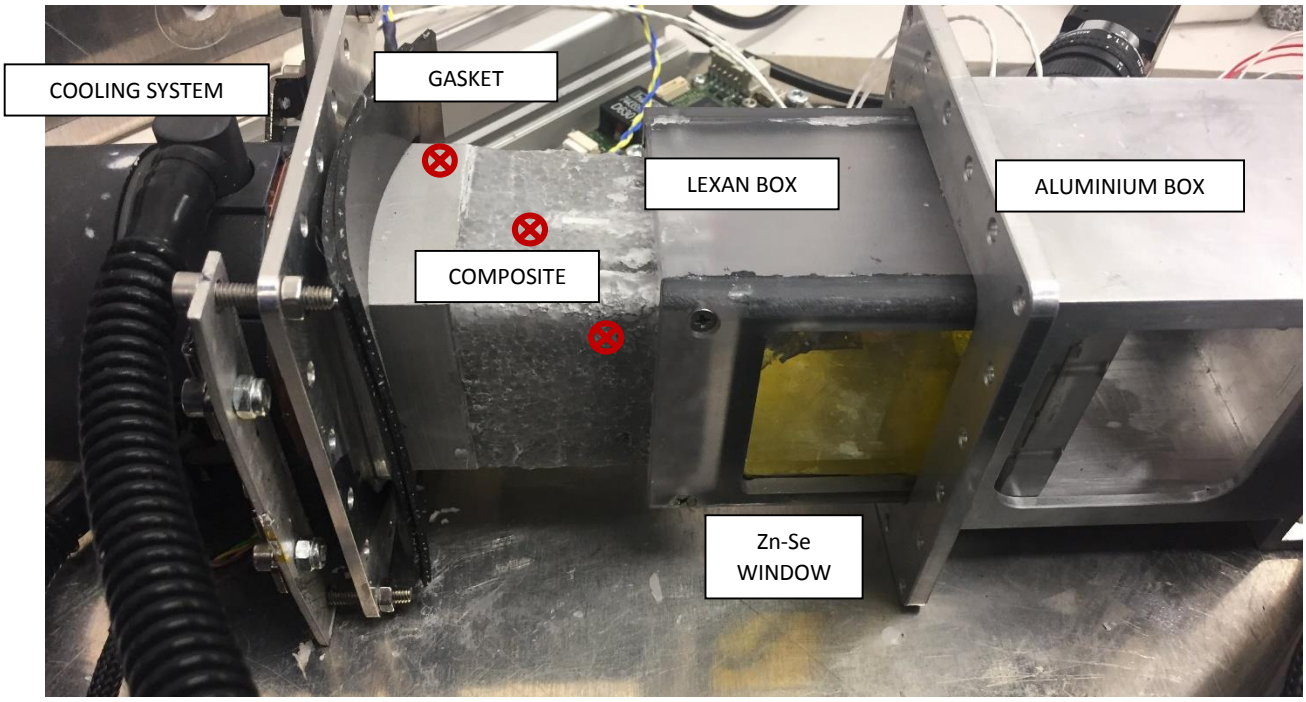

Fig. 2 - Experiment schematic representation

The Peltier cell during heating can deliver 80 W. Liquid paraffin wax fills aluminum foam with roughly 95/97% filling ratio. Sizes of PCM/foam device are 50x50x50 mm, as already mentioned in the 2D numerical model section. The device is laced in a polycarbonate box in order to appreciate melting and solidification process by means of a CMOS camera and with a Low Wave InfraRed (LWIR) camera FLIR ® A65. For this purpose, a Zn-Se window is placed. Black paint is used on aluminum foam surface to maximize absorbed radiation for imaging. Finally, in order to insulate aluminum plate from lexan box and to avoid paraffin leakage, a neoprene gasket is employed.

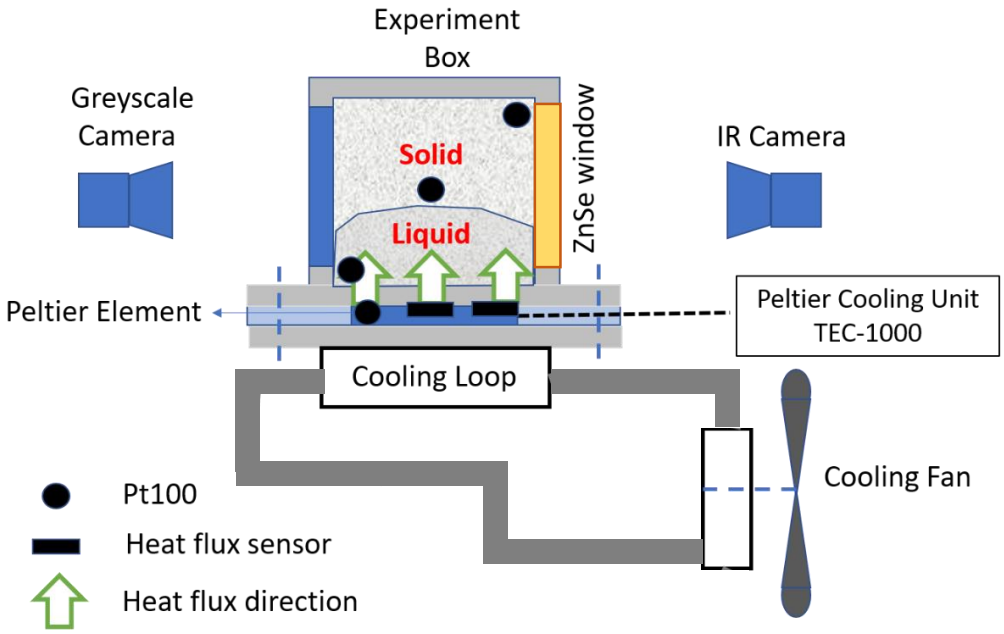

Fig. 3 - Experimental facility, global scheme, view from above.

A sketch of the system is shown in Fig. 3, including cameras, Zn-Se window and both heat flux sensor and Pt100 temperature sensor. It is evident from the figure that heat comes in the PCM/foam device from Peltier cooling unit TEC-1000, while this is cooled with a cooling loop to guarantee heat remove from Peltier cooling unit. Heat flux sensor present a ±0.1 W/cm^2 maximum error, while LWIR camera is calibrated by employing Pt100 temperature sensors. Maximum error achieved after calibration is ± 0.8 °C.
To track the melting front position, IR camera results are employed. Details of the procedure can be found in Filippeschi et al. [19] and these are briefly reported in the following. First of all, IR images have to be used instead of greyscale images because with greyscale images there are three different color gradations that are light and dark grey, referred to liquid and solid PCM, respectively, and a bright grey that is the foam. Because of this, greyscale images cannot be used to establish melting front. The melting zone is established starting from temperature measurements. After melting temperature range and zone are established from IR images, one can perform a second-order polynomial interpolation on the melting zone to dump local temperature oscillations. The fitted curve corresponds to the melting interface.

4. Results and comparisons

4.1 Comparisons with experiments

4.1.1 Vertical orientation

Experiments reported in Table 3 are here performed in order to appreciate porosity, PPI and orientation effects. Heat fluxes reported are both referred to Peltier cell (q_{Pelt}, 16 cm^2 heat transfer area) and PCM with foam (q_{in}, 25 cm^2 heat transfer area). In this contribution, both vertical and horizontal orientation are investigated, in order to appreciate gravity direction effect. All the experiments are compared with numerical simulations to guarantee code accuracy. In all the cases, $t = t_m$ is set as the time at which melting begins In Figs. 4-6, melting front evolution with time is presented for both experimental and numerical approaches for experiments #2, #4 and #8, that present different PPIs.. Generally, a good agreement has been found between the two approaches. With references to vertical orientation, in all the cases the melting front looks to be differently shaped. The numerical simulations melting front shows a larger melted PCM area at the top of the domain. This could be due to the internal convection motion and the boundary conditions without any mass exchange. The melted PCM liquid is so stored in top part of the domain for vertical orientation. When foam is included, convection motions are damped with respect to pure PCM because of the role of the solid matrix that enhances the overall thermal conductivity, as also evident from [5, 8, 11], and the effectivity viscosity as well. In all the experiments, slight deviation in the extremities of the melting front might be attributed to convection dispersions to the environment and these will be discussed later. In spite of a slight melting front shape discrepancy the calculated and measured melting area can be compared with a good accordance.
A further comparison has been done on the PPI effect on the melting front. The code is capable of catch the effect for the PPI and the melting areas are comparable with the results coming from the experimental activity. In particular, , Experiments #2, #4 and #8 can be compared in terms of different PPIs (respectively, 40, 20 and 10) with all the other input variables fixed as evident from Table 3. Another qualitative effect on the melting front shape can be discussed here. It is possible to appreciate that with lower PPIs there is a slight enhancement of the melting zone in the top of the domain fo the vertical orientation because of the increase of natural convection motion. Indeed, lower PPIs means that pores are larger to allow liquid PCM movement, as already evident from [6]. This can be also evident from permeability K equation presented in Table 2 (from Calmidi [26]), where permeability increases with cell size.

Table 3 – Experiments here performed where (H) and (V) stands for horizontal and vertical, respectively

Experiment	q_{Pelt} (W/cm^2)	q_{in} (W/cm^2)	ε	PPI	Configuration
1	1.8	1.152	0.88	40	(H)
2	1.8	1.152	0.88	40	(V)
3	1.8	1.152	0.88	20	(H)
4	1.7	1.088	0.88	20	(V)
5	1.8	1.152	0.88	10	(H)
6	0.9	0.576	0.88	10	(H)
7	0.9	0.576	0.88	10	(V)
8	1.7	1.088	0.88	10	(V)
9	1.5	0.960	0.92	10	(H)
10	1.5	0.960	0.92	10	(V)
11	1.4	0.896	0.95	10	(H)
12	1.4	0.896	0.95	10	(V)

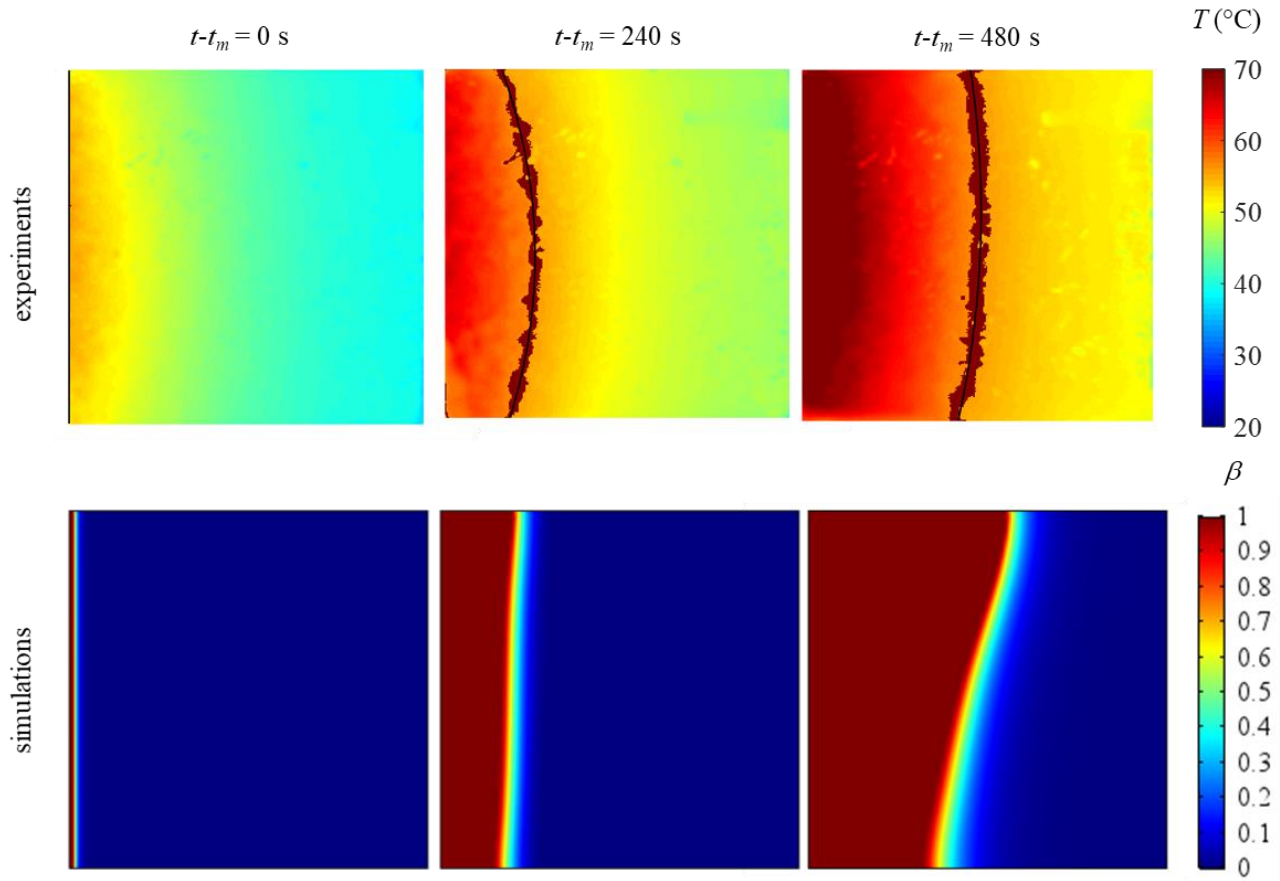

Fig. 4 - Temperature and volume fraction of experiments (top) and simulations (bottom) for experiment #2 (q_{Pelt} = 1.80 W/cm^2, ε = 0.88, PPI = 40 and vertical (V) configuration)

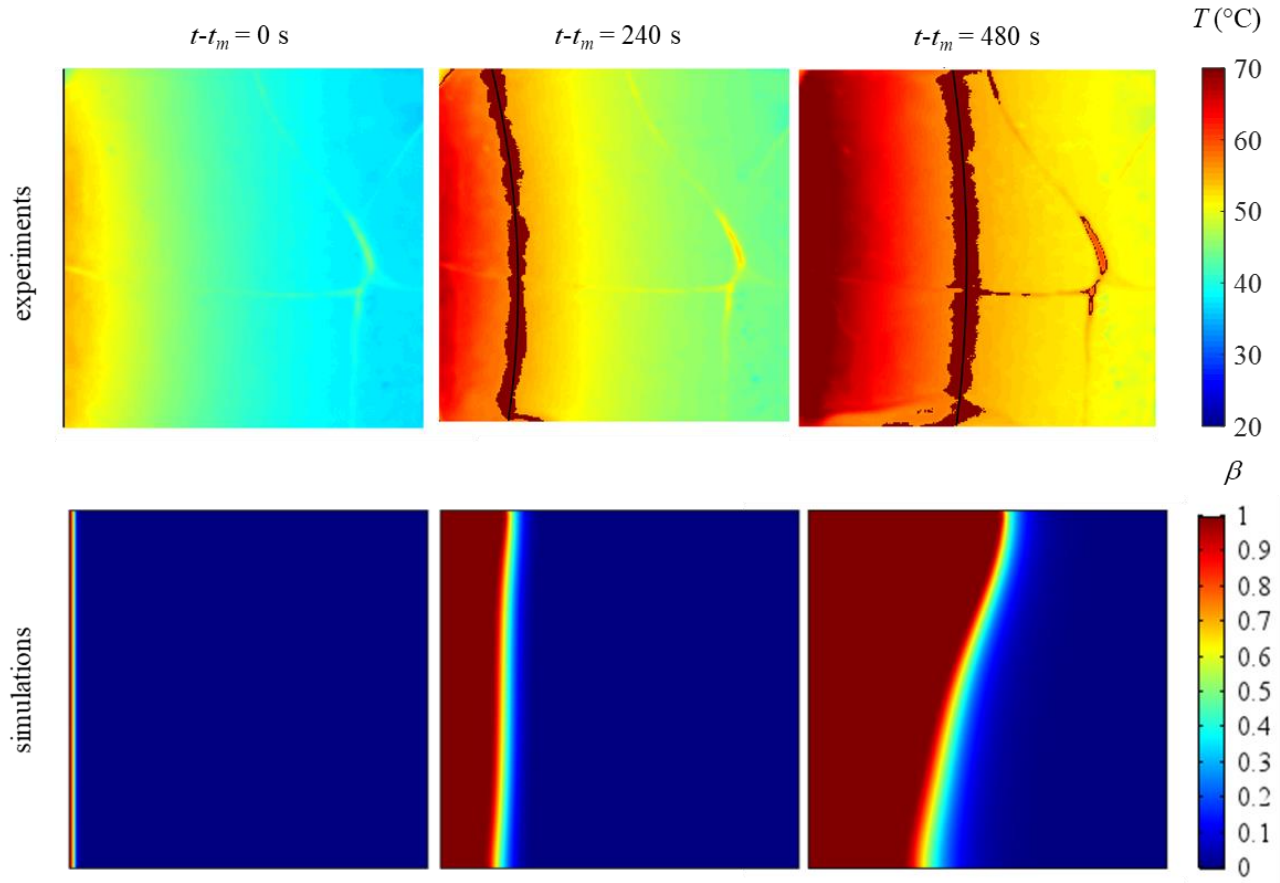

Fig. 5 - Temperature and volume fraction of experiments (top) and simulations (bottom) for experiment #4 (q_{Pelt} = 1.70 W/cm^2, ε = 0.88, PPI = 20 and vertical (V) configuration)

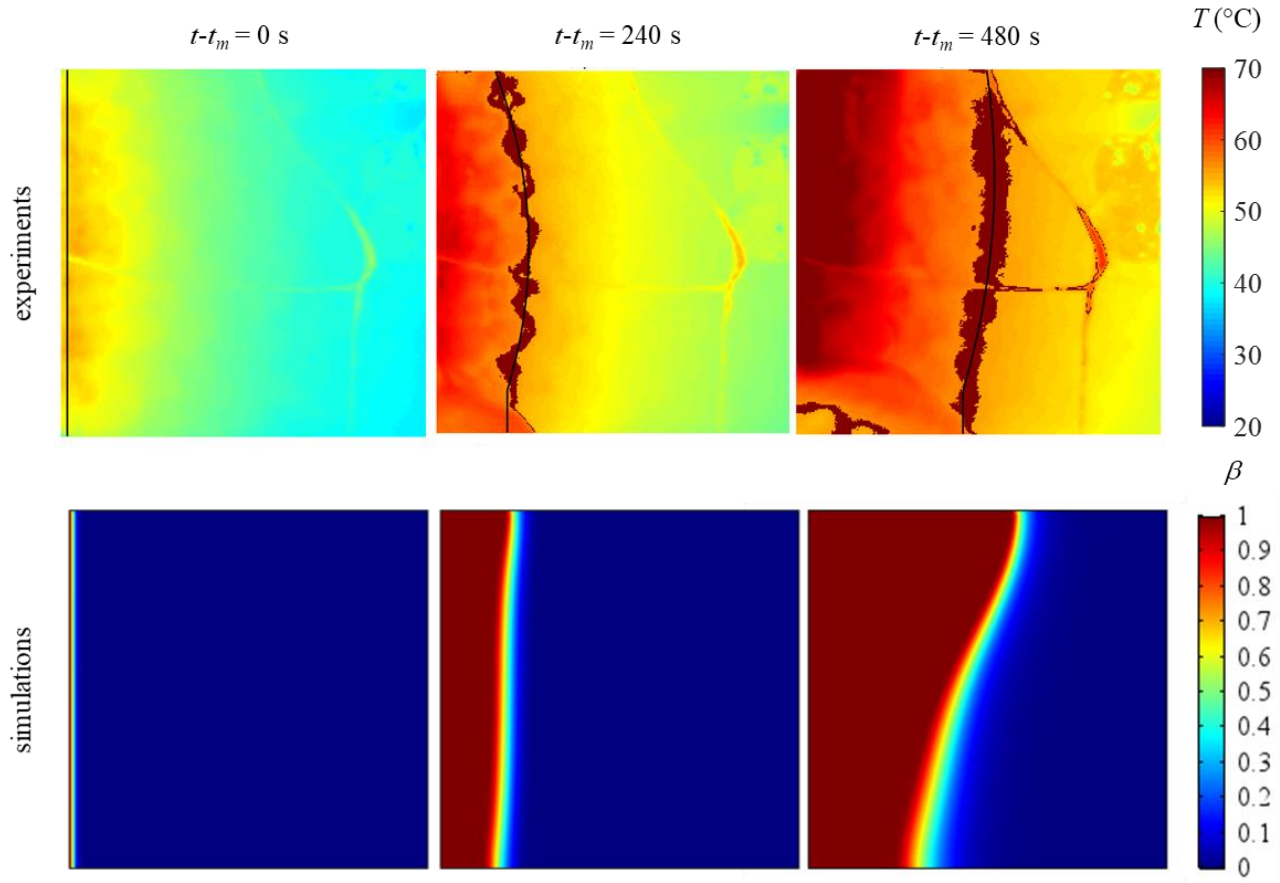

Fig. 6 - Temperature and volume fraction of experiments (top) and simulations (bottom) for experiment #8 (q_{Pelt} = 1.70 W/cm^2, ε = 0.88, PPI = 10 and vertical (V) configuration)

On the other hand, porosity effect can be observed by comparing experiments #8 (Fig. 6) with #10 and #12 (Figs. 7 and 8), that are foams with different porosity and equal PPIs (0.88, 0.92 and 0.95 respectively). It is shown that higher porosity makes melting front more curved because of lower foam thermal conductivity (see Table 2 [30]), making conduction less important than convection.

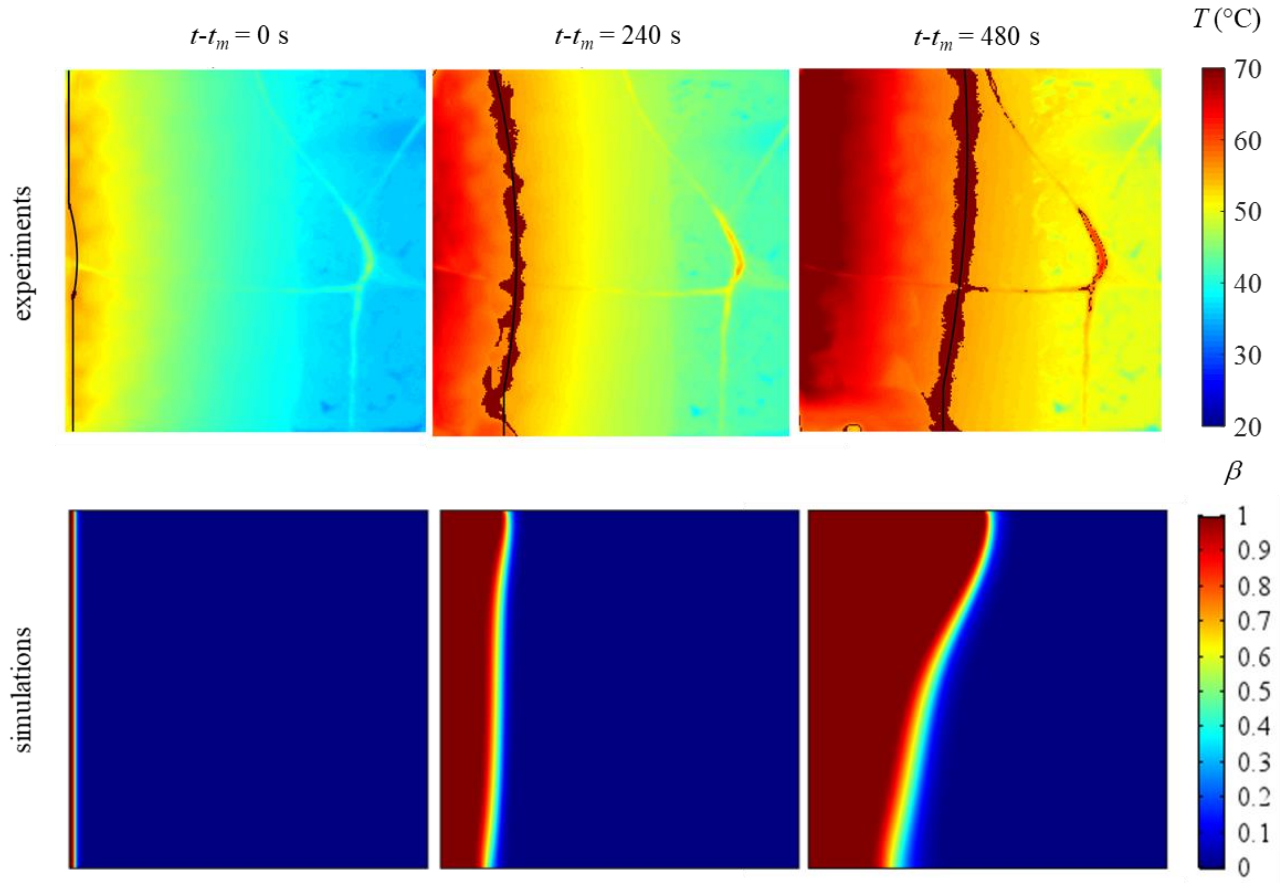

Fig. 7 - Temperature and volume fraction of experiments (top) and simulations (bottom) for experiment #10 (q_{Pelt} = 1.50 W/cm^2, ε = 0.92, PPI = 10 and vertical (V) configuration)

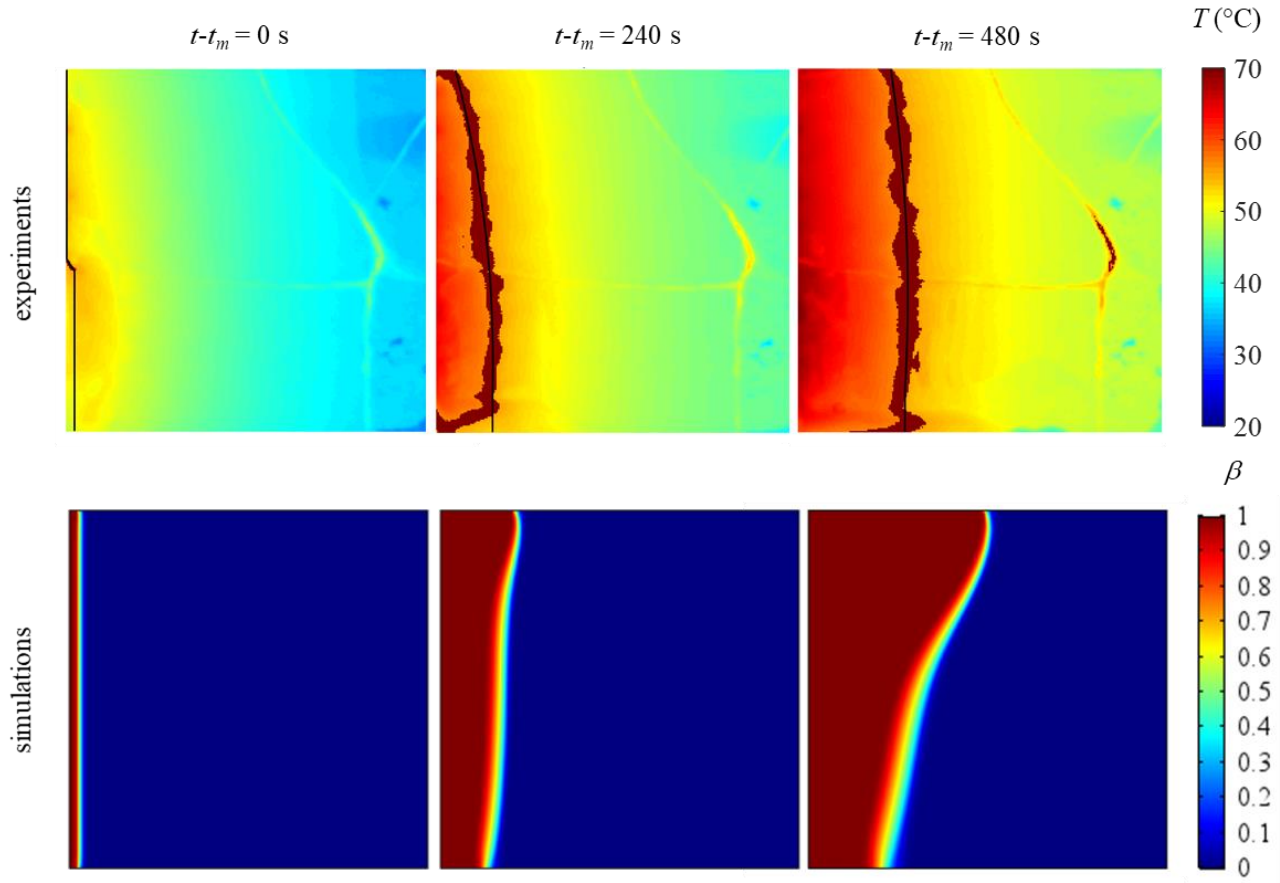

Fig. 8 - Temperature and volume fraction of experiments (top) and simulations (bottom) for experiment #12 (q_{Pelt} = 1.40 W/cm^2, ε = 0.95, PPI = 10 and vertical (V) configuration)

4.1.2 Horizontal orientation

With references to horizontal orientation, a even better agreement between experiments and simulations has been found. Melting fraction function for both experimental and numerical results referred to experiments #1, #3 and #5 are presented in Figs. 9-11. Generally, with respect to the vertical orientation the numerical melting front looks more uniform respect to the gravity orientation because of the different behavior of natural convection motions. The role of PPI on the melting front shape shows similar results. Experiments #1, #3 and #5 show different PPIs behavior at the same porosity. No remarkable differences can be found since there is no relevant convection, thus the problem is mainly conductive and overall thermal conductivity is not affected by PPIs (see Table 2).

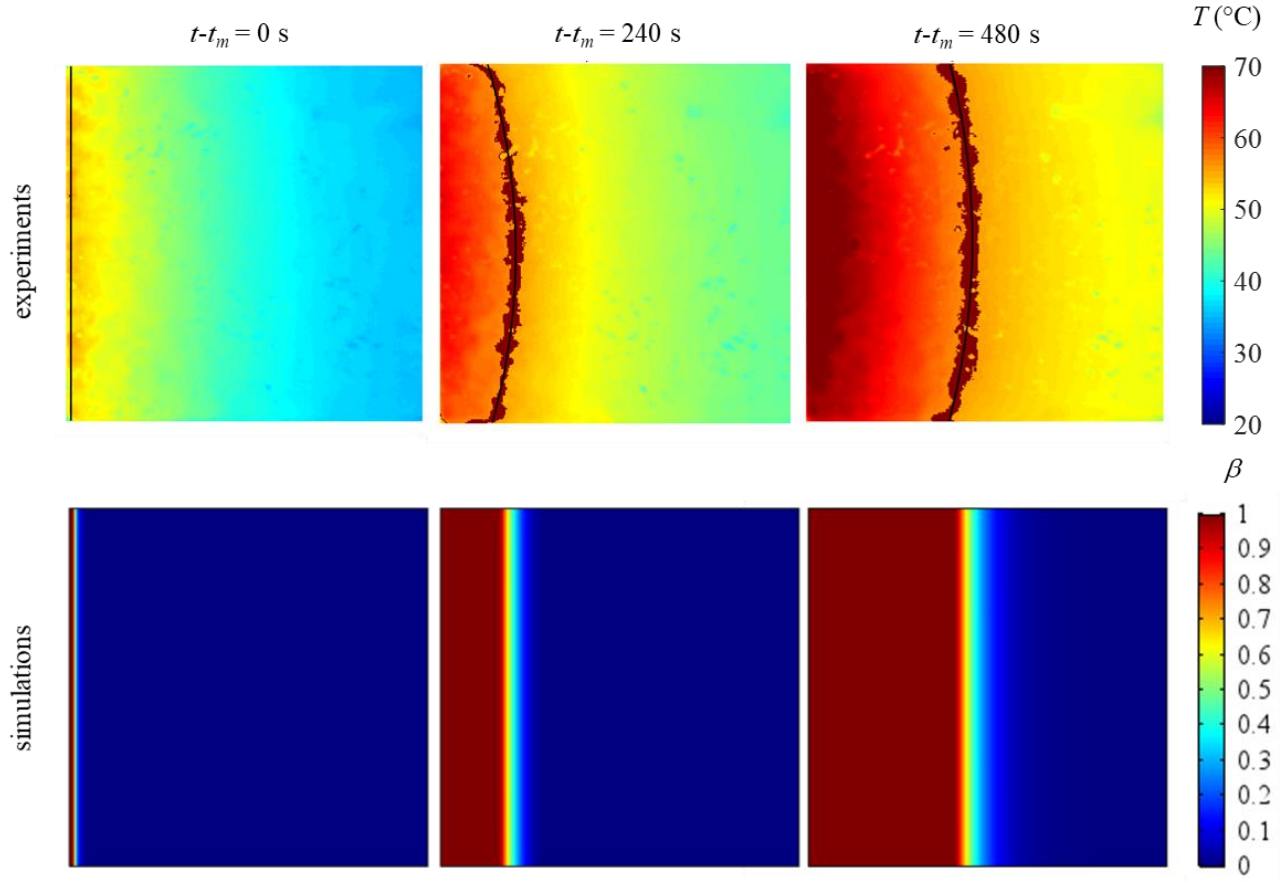

Fig. 9 - Temperature and volume fraction of experiments (top) and simulations (bottom) for experiment #1 (q_{Pelt} = 1.80 W/cm^2, ε = 0.88, PPI = 40 and horizontal (H) configuration)

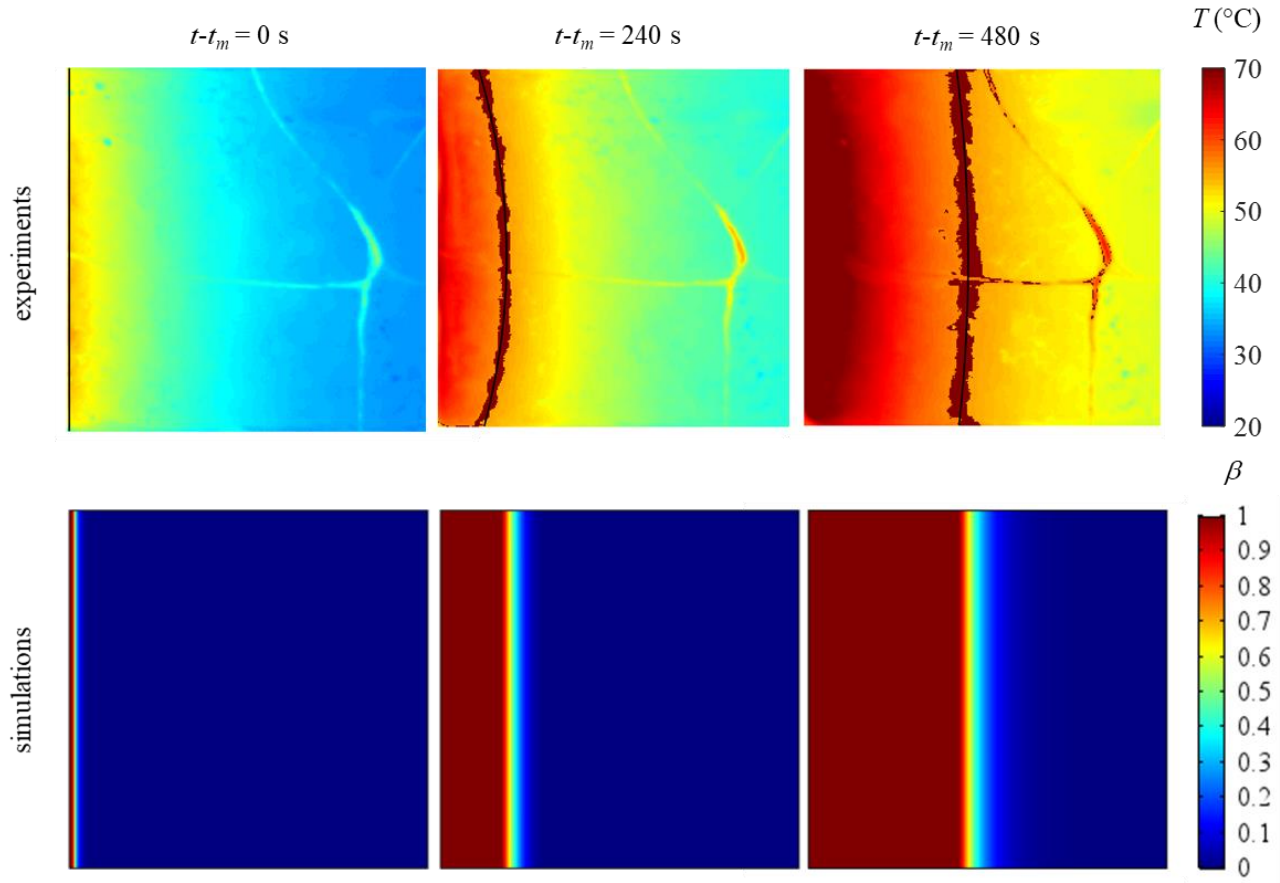

Fig. 10 - Temperature and volume fraction of experiments (top) and simulations (bottom) for experiment #3 (q_{Pelt} = 1.80 W/cm^2, ε = 0.88, PPI = 20 and horizontal (H) configuration)

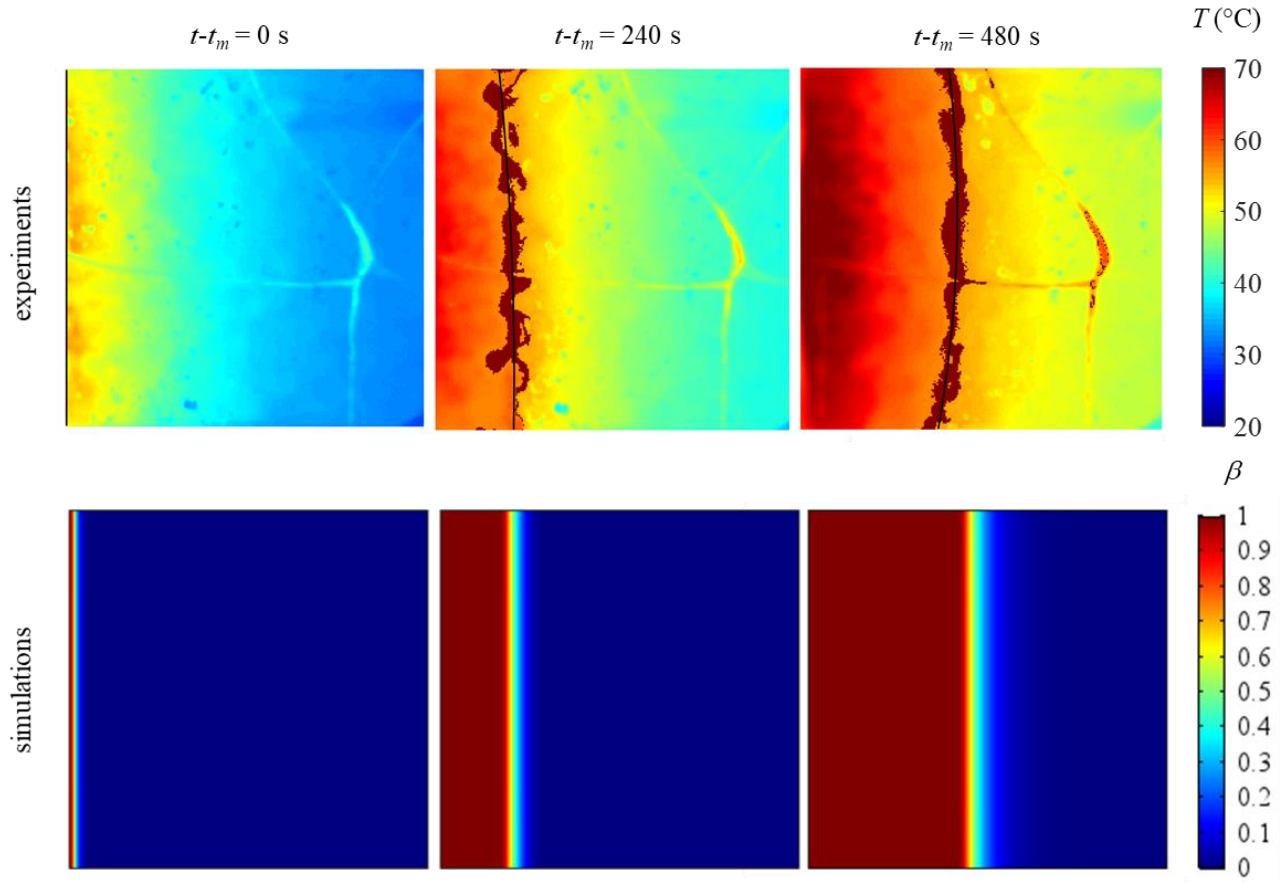

Fig. 11 - Temperature and volume fraction of experiments (top) and simulations (bottom) for experiment #5 (q_{Pelt} = 1.80 W/cm^2, ε = 0.88, PPI = 10 and horizontal (H) configuration)

The porosity effect in case of to horizontal orientation are analyzed by comparing experiment #5 (Fig. 11) with experiments #9 and #11 (Figs. 12 and 13), thus porosities of 0.88, 0.92 and 0.95 are compared. where results thatthe lower the porosity the faster is the melting front due to the higher convection. The role of convection has been numerically shown in Fig. 14 for experiment #11. Rayleigh-Benard cells are evident in this figure. This happens because at higher porosities thermal conductivity effects becomes less important on natural convection motion. However, is important to underline that such effects were not remarkable for experiments probably because of convection heat losses at the boundaries or because of an inaccurate evaluation of the effective viscosity.

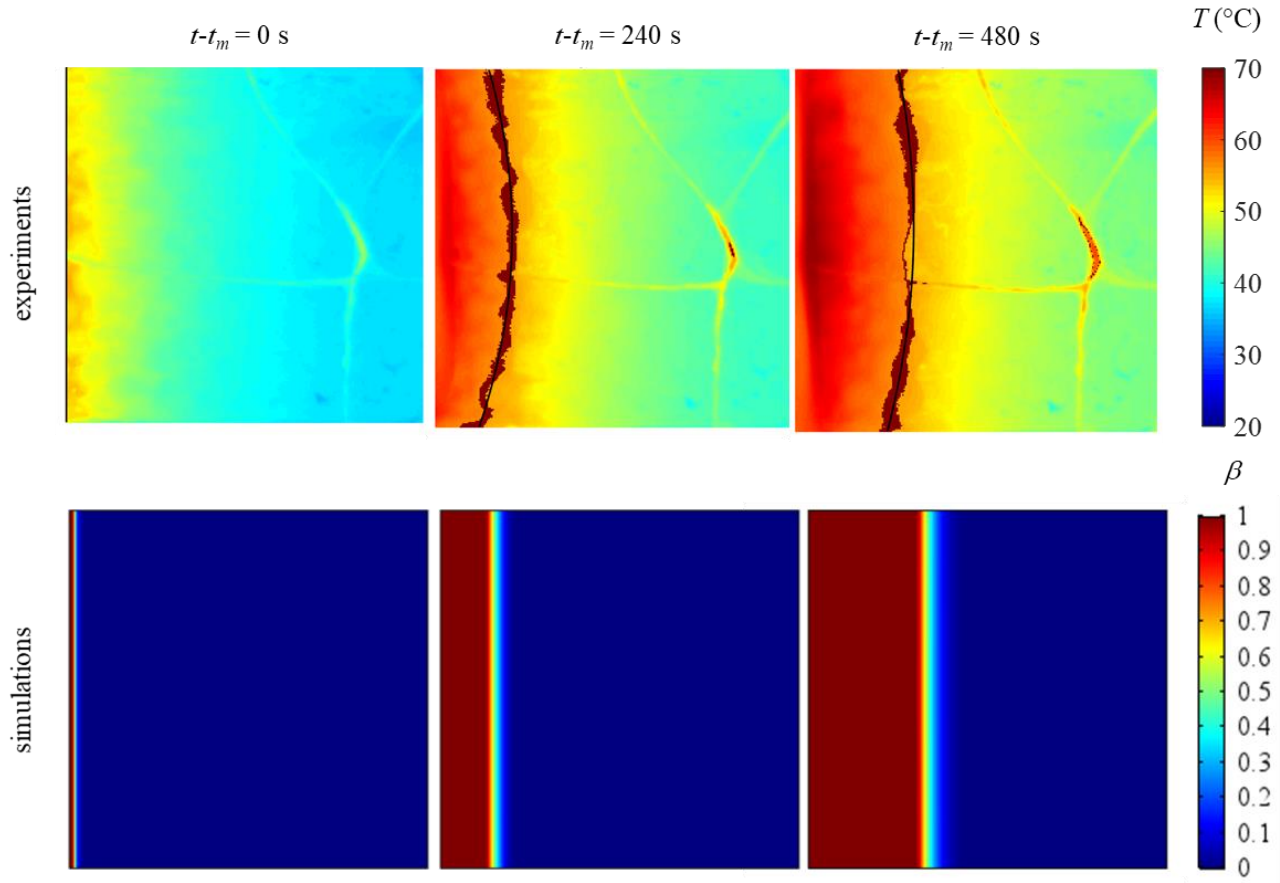

Fig. 12 - Temperature and volume fraction of experiments (top) and simulations (bottom) for experiment #9 (q_{Pelt} = 1.50 W/cm^2, ε = 0.92, PPI = 10 and horizontal (H) configuration)

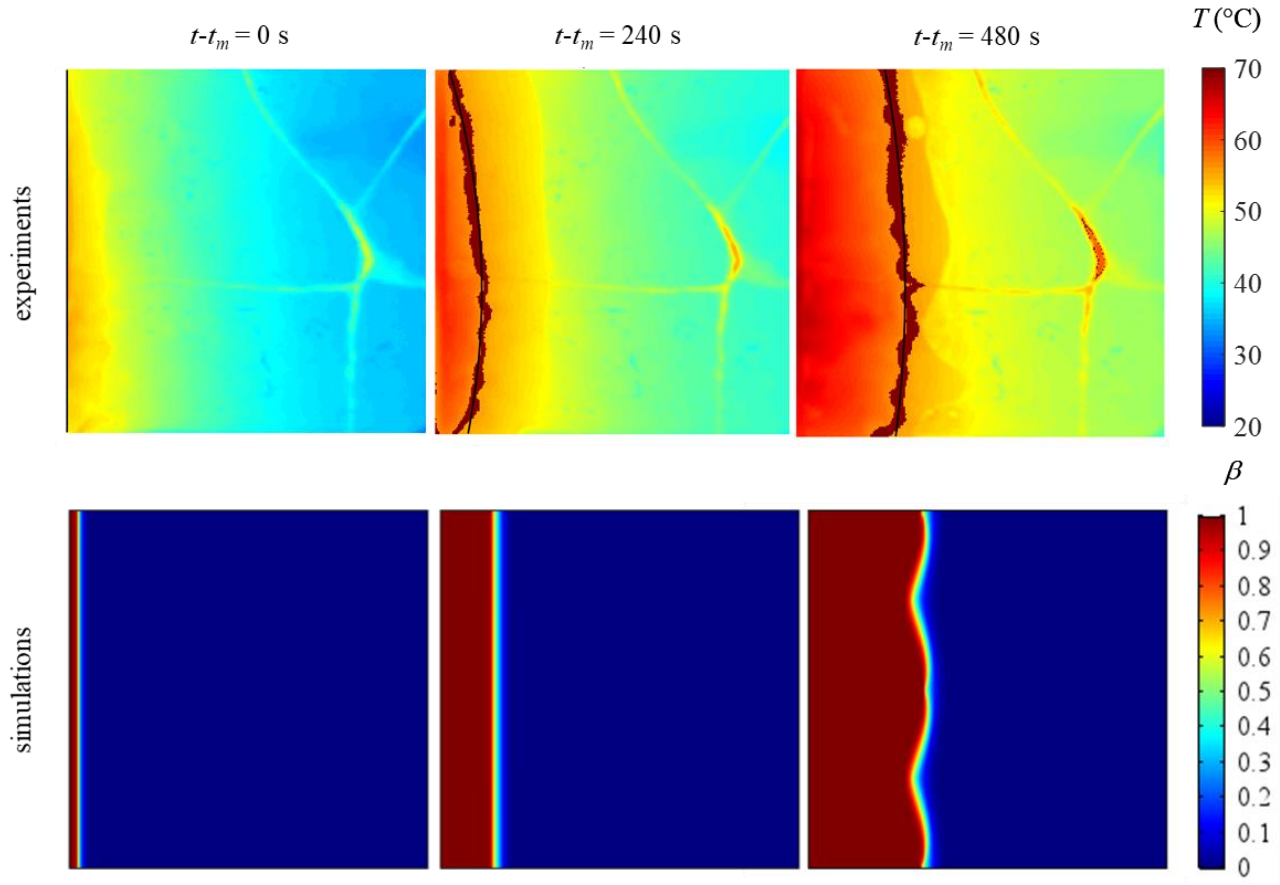

Fig. 13 - Temperature and volume fraction of experiments (top) and simulations (bottom) for experiment #11 (q_{Pelt} = 1.40 W/cm^2, ε = 0.95, PPI = 10 and horizontal (H) configuration)

4.2 Velocity and temperature fields

To appreciate convection effects, velocity fields and vectors are reported in Figs. (14) and (15) for both vertical and horizontal configurations. In all the cases, it is reminded that the velocity solution in the solid phase is forced to approach zero because a fixed-grid method is here employed. For the vertical configuration, experiments #2 and #8 (Figs. 14a and 14c) and #8 and #12 (Figs. 14b and 14d) are compared to appreciate the PPI f PPIs and porosity effects. Typical convection motions with a core at lower velocity is shown in all cases, while maximum velocities are achieved in the peripheries of the liquid, especially near the solid/liquid boundary. With references to PPI effect (Figs. 14a) and 14c)), one can remark that at lower PPIs (say, 10) velocities are slightly higher, with a slightly higher distortion of the front caused by a more vigorous motion. As already mentioned, this happens because of reduced permeability for lower PPIs, that makes easier for the liquid to pass through foam pores. Porosity effect highlighted in Figs. 14b and 14d showed that at higher porosity melting front is slower because of reduced overall thermal conduction in the solid phase. In the liquid region, one can remark that velocities achieved are slightly higher than for the other case because of the higher permeability for the higher porosity (see permeability K equation in Table 2 [26]).
In order to appreciate differences between vertical and horizontal configurations, velocity fields are presented in Fig. (15) for experiments #5 and #8 (Figs. 15a and 15c) and 11 and 12 (Figs. 15b and 15d). First, it is shown that for the horizontal configuration (Figs. 15a and 15b) typical convection motion cores can be distinguished, and two zones are created by recirculation. The higher the porosity, the slower is the melting front, but more liquid cores can be

distinguished. When the two configurations are compared, it is sown that melting front has a completely different behavior.

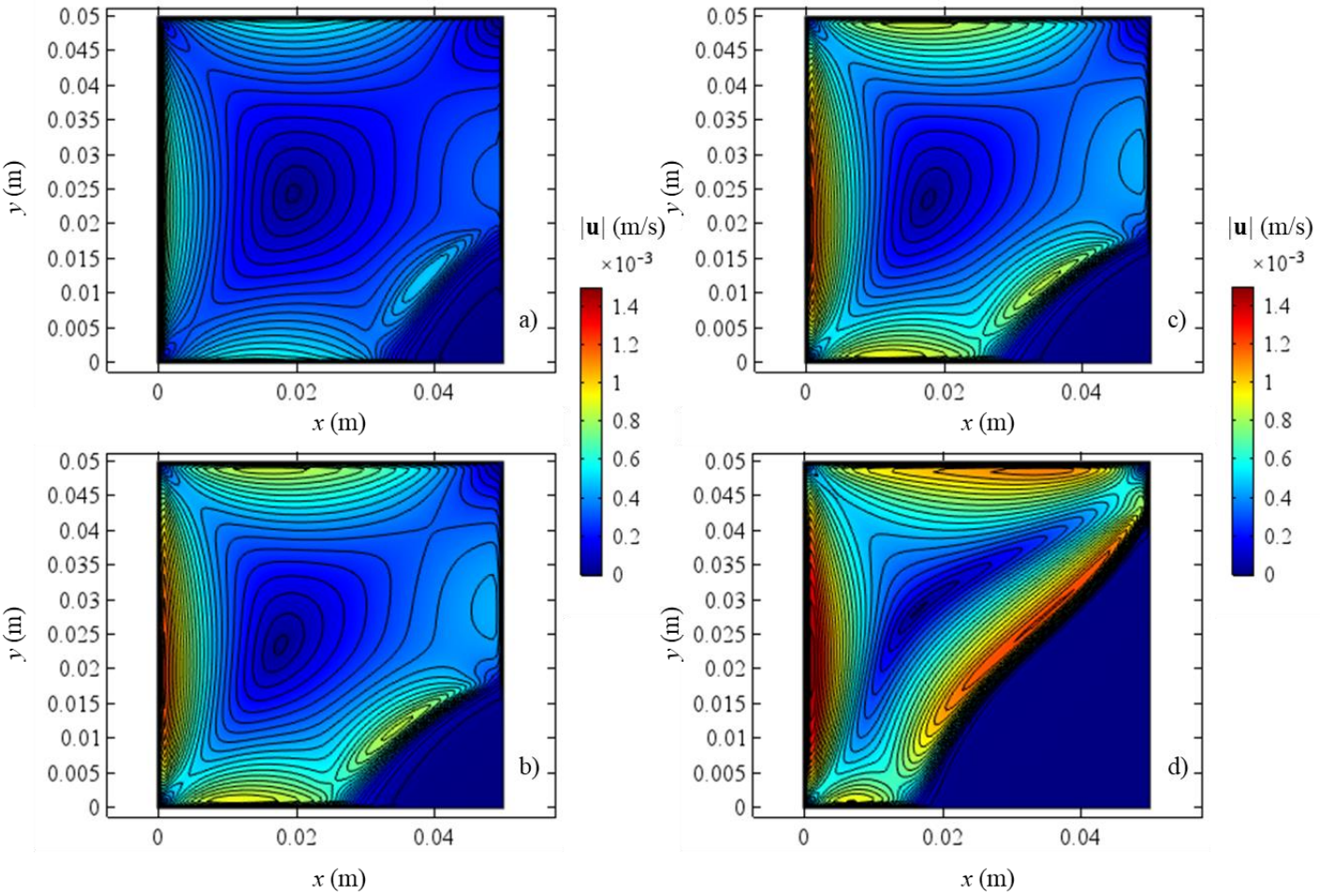

Fig. 14 - Velocities for a) experiment #2, b) and c) experiment #8, and d) experiment #12, at t-t_m = 840 s

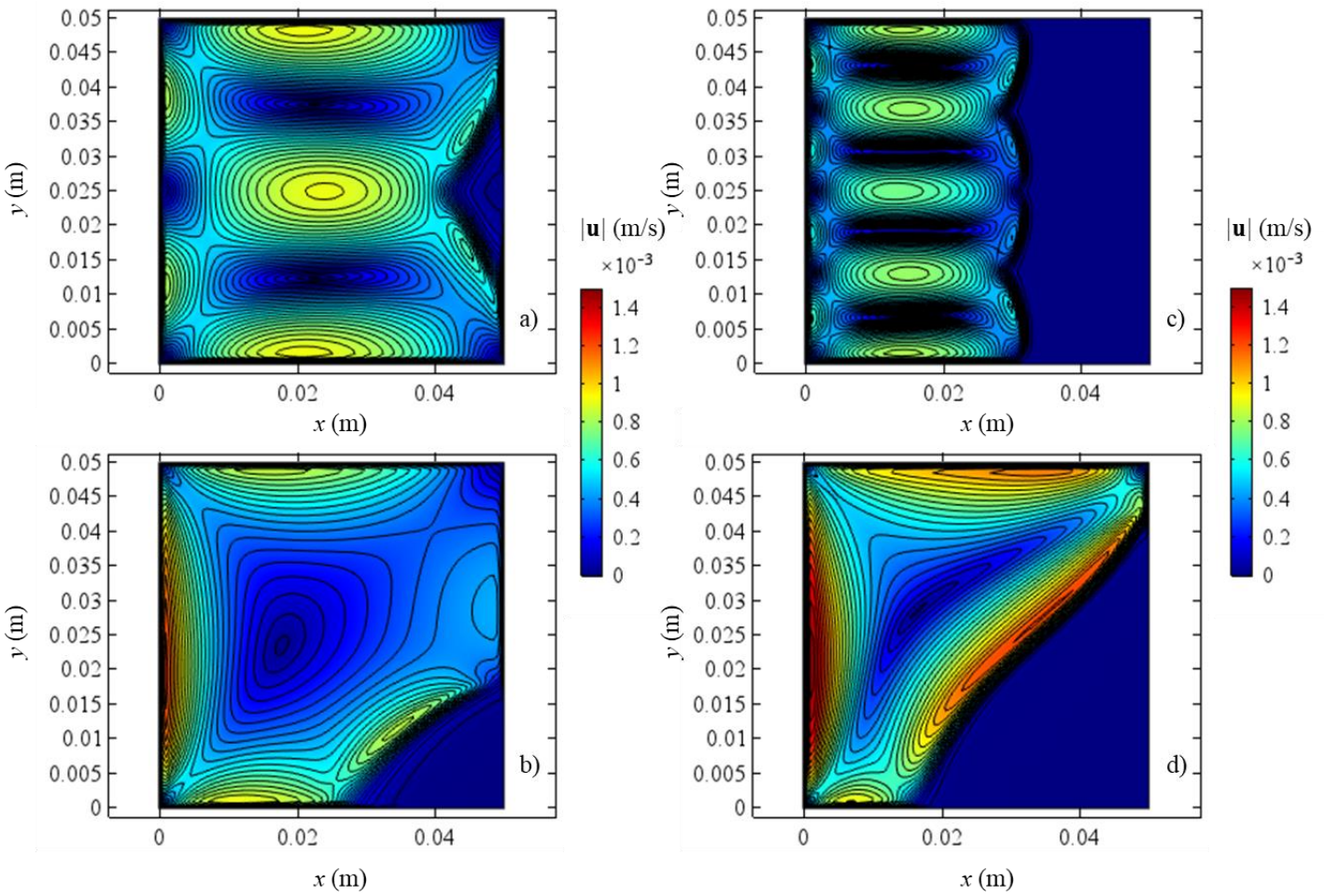

Fig. 15 - Velocities for a) experiment #5, b) experiment #8, c) experiment #11 and d) experiment #12, at t-t_m = 840 s

Temperature evolution of both phases are now shown. A sketch of temperature maps for both PCM and foam phases is presented in Fig. (16) for experiments #4 and #11, that present equal foam characteristics but different orientations. In all the cases, melting front distortion caused by convection makes isothermal lines to not be orthogonal to the applied heat flux. For the vertical orientation (Figs. 16a and 16c), higher temperatures are achieved in the top side because of natural convection, while for horizontal orientation (Figs. 16b and 16d) natural convection makes higher temperatures to not be achieved in the middle of the domain (say, for $y = L/2$) because of typical convection motion, already analyzed in Fig. (15).

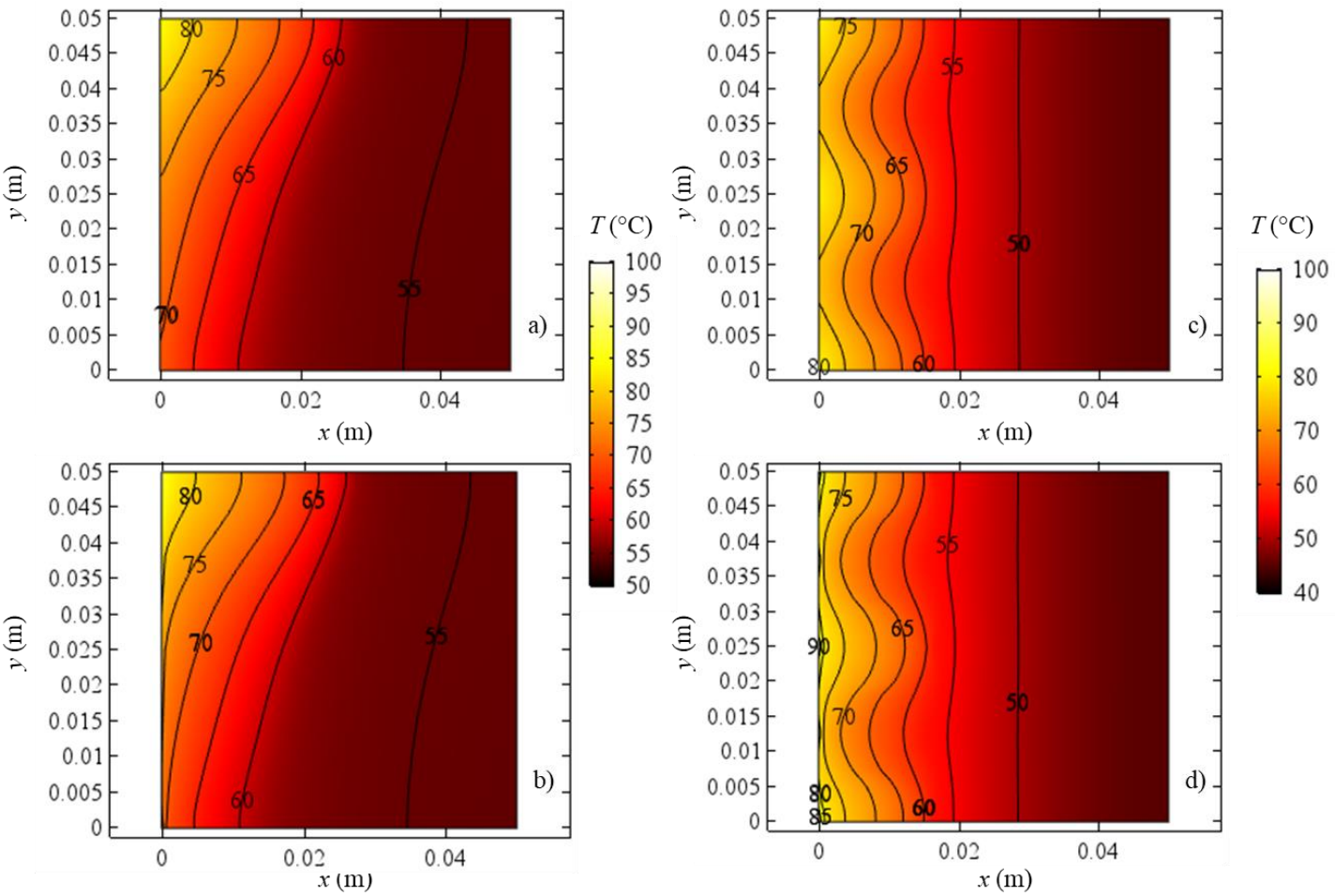

Fig. 16 - a) foam and b) PCM Temperature fields for experiment #4, and c) foam and d) PCM Temperature fields for experiment #11, at t-t_m = 480 s

Finally, with references to PCM and foam phases, it is shown that these are not equal everywhere because of LTNE effects. The importance of such effects has been analyzed previously by Zhang et al. [18]. They showed that temperature differences can be about 3 °C, with high differences achieved in the proximity of the mushy zone. LTNE effects are analyzed in detail in Fig. (17). It is shown that in most of the domain PCM and foam present the same temperature because LTE is achieved. This has been also pointed out by Feng et al. [32], while Yang et al. [12] reported that local thermal equilibrium is reliable with Stefan numbers lower than 0.22. However, it is important to underline that LTNE effects are important in the proximity of the applied heat flux, where such differences can reach about 12 °C in the present case. This because of the heat flux bifurcation that happens between the two phases of the porous domain (say, PCM and foam). In this paper, it is assumed that heat flux is split in the two phases as a purely parallel heat transfer, weighted on porosity definition (see Eqs. 7a-b). Thus, the reaction of the two materials in the proximity of the applied heat flux is different, while in the other region they reach local thermal equilibrium because of the interfacial convective heat transfer. Finally, it is important to remark that small local thermal non equilibrium effects might arise in some points of the liquid regions. For example, with references to the horizontal configuration with 10 PPI and 0.95 porosity (Fig. 17d), one can observe that temperature differences could be about 3 to 4 °C in the core region.

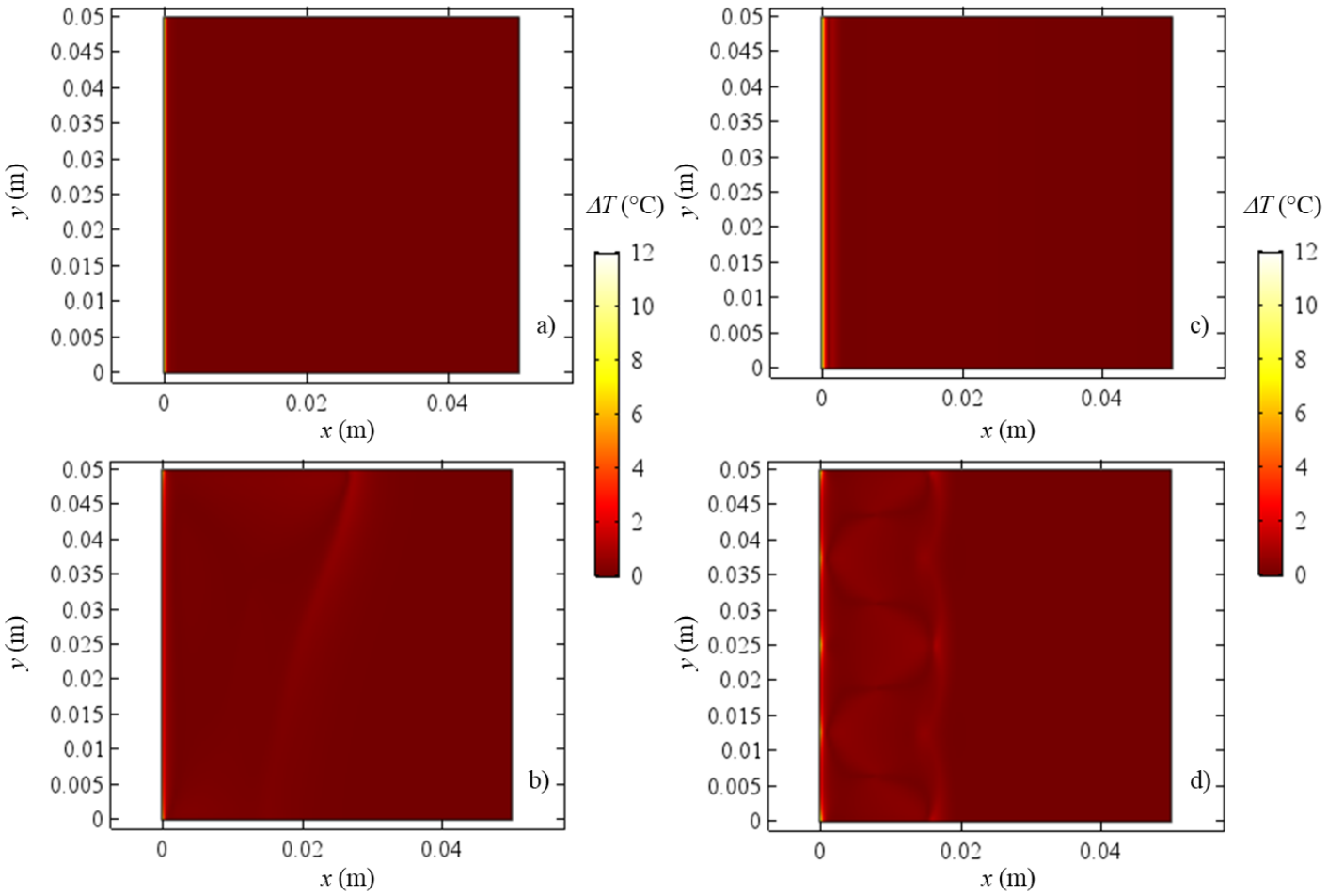

Fig. 17 - Temperature difference between PCM and foam for experiment #4: a) t-t_m = 0 s and b) t-t_m = 480 s, and for experiment #11: c) t-t_m = 0 s and d) t-t_m = 480 s

4.3 Effects of melting temperature and convective external dispersion

As already reported, external dispersion due to convection might arise. As an example, experiment #7 simulations have ben ran by assuming a convection dispersion with different heat transfer coefficients (say, h = 0, 10 and 20 W/m^2 K) and ambient temperatures (equal to the initial temperature) for both the top and the bottom of the domain. In particular, thermal dispersion is referred only to the foam, while adiabatic assumption is still done for the PCM equation. Such simulations are shown in Fig. (18). It is shown that with no dispersion (h = 0 W/m^2 K), even if front position is similar the simulation gives a slight distortion of the front due to natural convection, that is not shown in the experiments. However, is evident that the higher the heat transfer coefficient in the simulations, the more the profile becomes distorted. For h = 20 W/m^2 K, profile becomes qualitatively similar to the one achieved in the experiments, which means that heat dispersions a variable that should be considered when modeling PCM with foams. The slightly different position of the melting front in the simulations can be attributed to the non-perfectly steady heat flux applied, which present a slight variation with time that here we assume to be negligible.

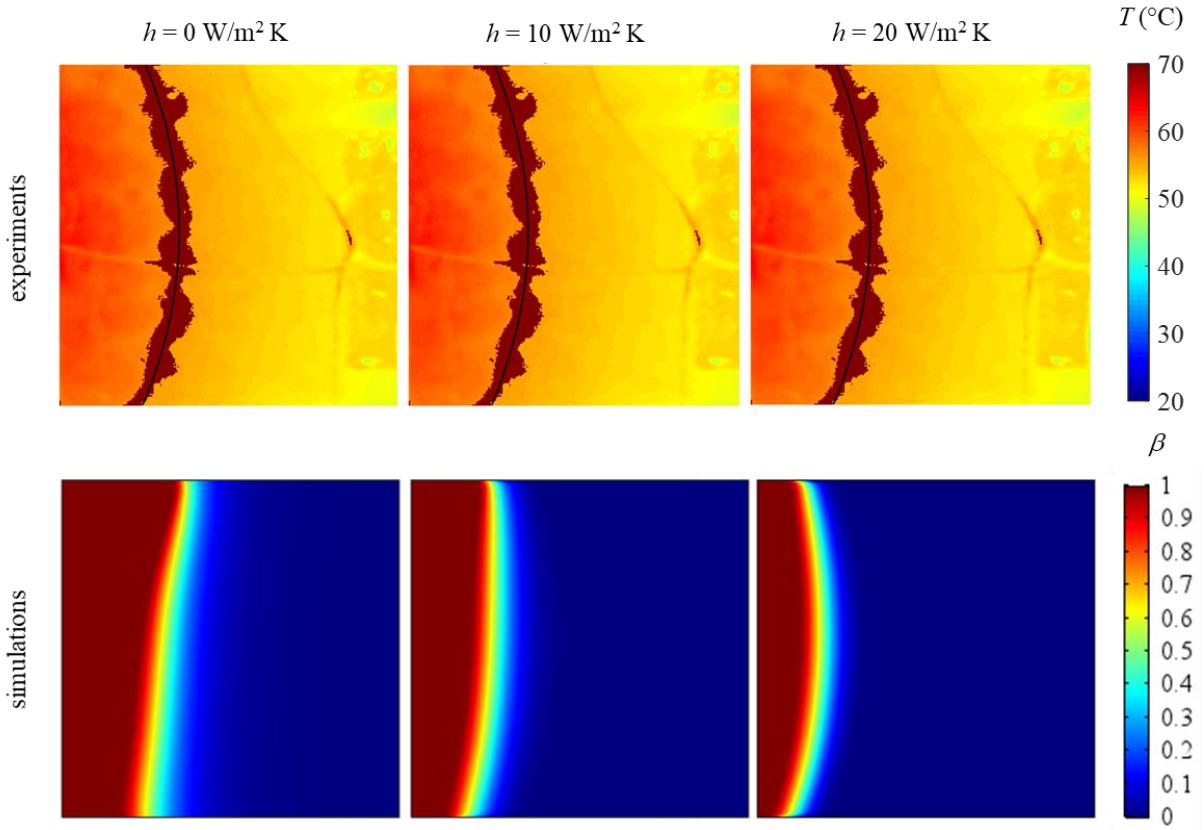

Fig. 18 - Melting fraction functions for experiment #7 with different values of the exterior heat transfer coefficient h, at t-t_m = 840 s

Another variable that is relevant is the melting temperature difference. With references to experiment #7, different melting temperatures have been compared (from 0.5 °C to 5 °C) and presented in Fig. (20). It is shown that melting front is qualitatively in the same position, but mushy zone extension becomes higher in all the cases.

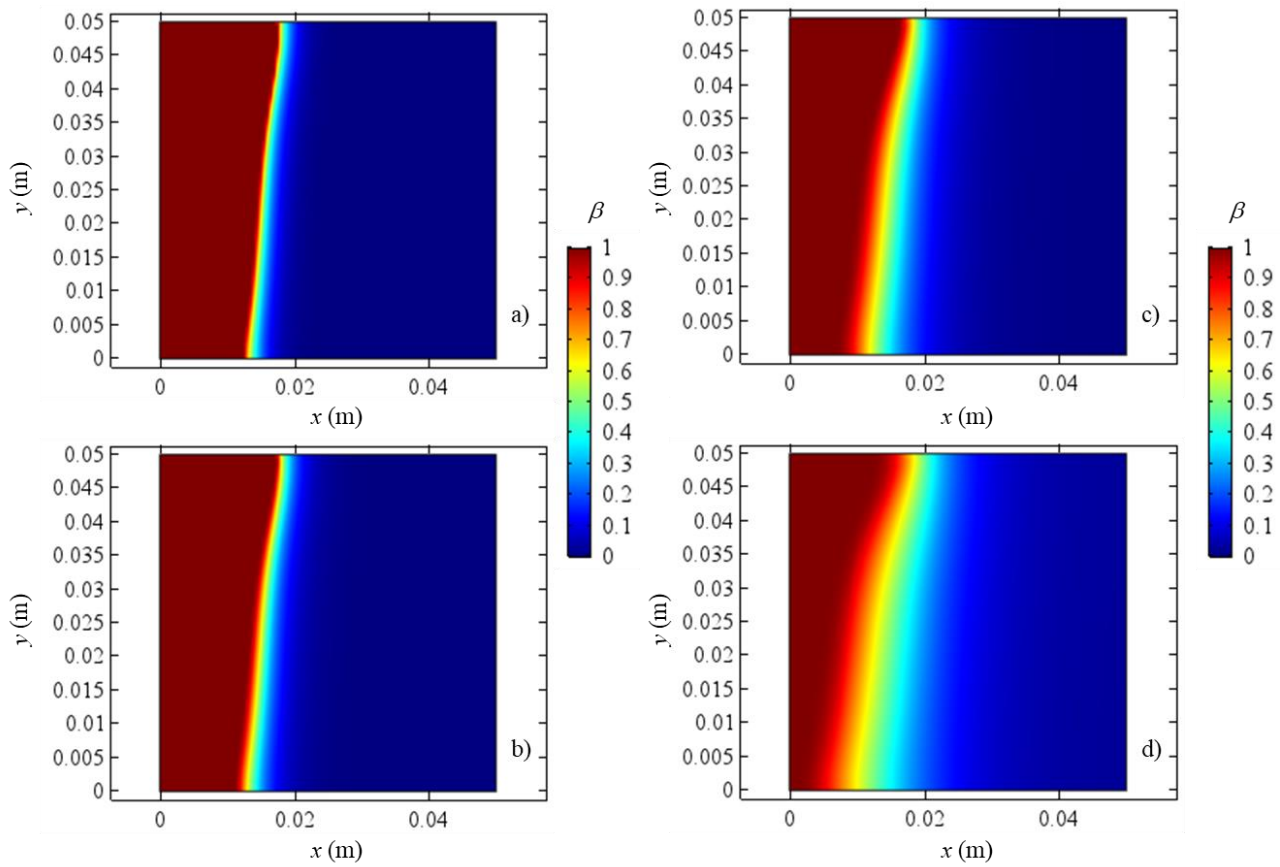

Fig. 19 - Melting fraction functions for experiment #7 with a) ΔT_m = 0.5 °C b) ΔT_m = 1.0 °C, c) ΔT_m = 2.5 °C and d) ΔT_m = 5.0 °C, at t-t_m = 840 s

4.4 Total melting fractions

When PCMs are modeled, it is fundamental to evaluate total melting fraction evolution, that is the integration of the variable β with time. Indeed, metal foam has the role of reducing total melting time. Comparisons between experiments and numerical simulations in terms of total melting fraction evolution vs. time is shown in Fig. 20. A good agreement between experiments and numerical simulations is shown. Negligible effects of PPIs can be found in both vertical (Fig. 20a) and horizontal (Fig. 21c) orientations. Effect of porosity are highlighted in Figs. (20b) and (20d) for both vertical and horizontal orientations, respectively. It is shown that higher total melting fractions can be achieved for lower porosity because of the enhanced overall thermal conductivity. Comparisons between horizontal and vertical configurations are shown in Fig. 21 for both PPIs (Fig. 21a) and porosity (Fig. 21b) effects. No relevant effects of the orientation have been found, except slight differences for ε = 0.95 (Fig. 21b), that can be attributed to the fact that for some cases natural convection can be significant for both horizontal and vertical configuration, as previously shown in Figs. 16-17. Besides, it is noticed that for this case applied heat flux is slightly different between ε = 0.88 and ε = 0.95, but conclusions here shown will be unaffected by this since lower porosity means higher total melting fraction (see Fig. 21b) as already shown in the literature survey (see for instance [5, 12]), thus in this figure the scope is to compare different orientation effects.

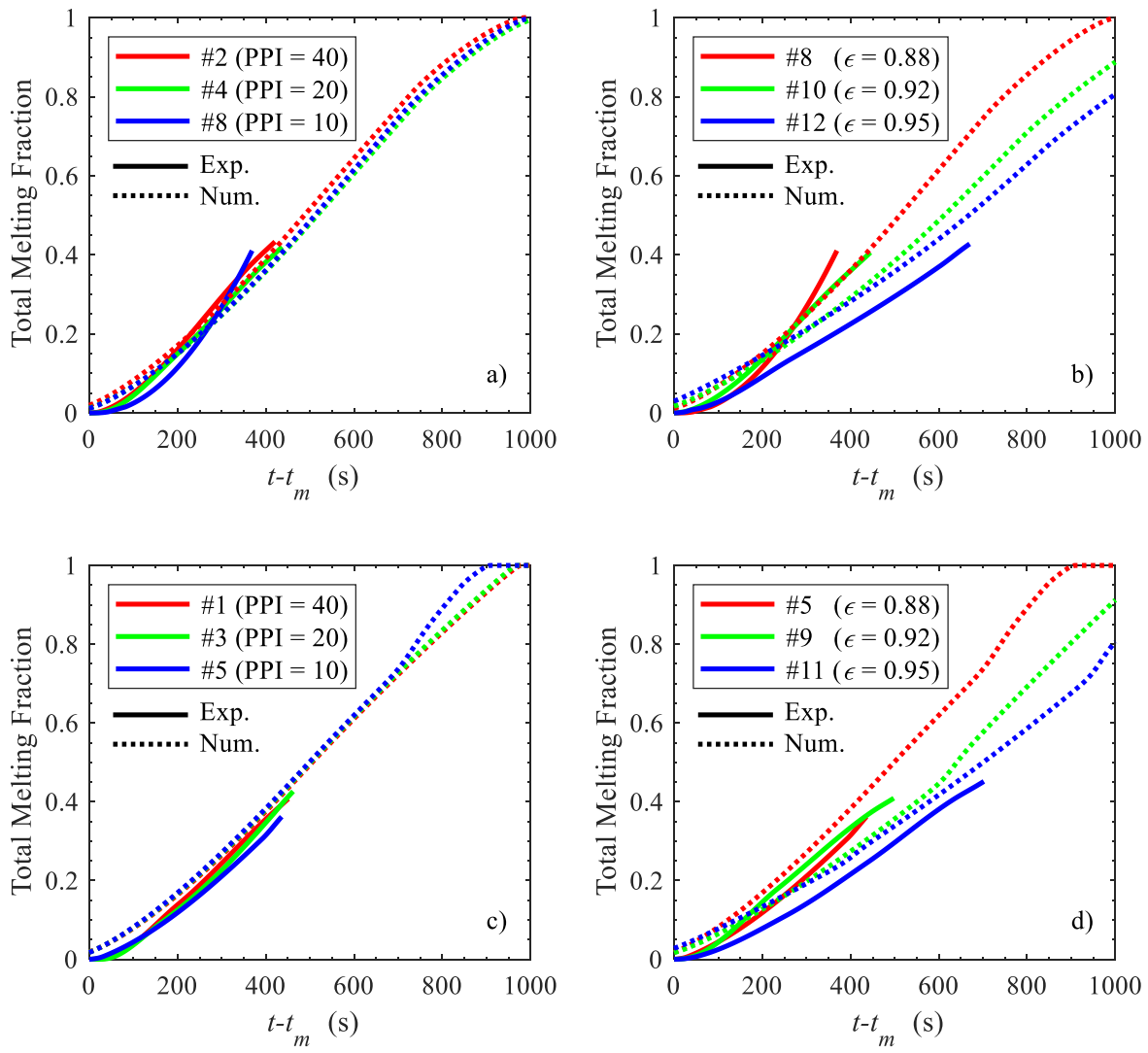

Fig. 20 – Total melting fractions evolution with time for both experimental (Exp.) and numerical (Num.) results: a) PPI effect with ε = 0.88 and vertical (V) configuration, b) porosity effect with PPI = 10 and vertical (V) configuration, c) PPI effect with ε = 0.88 and horizontal (H) configuration, and d) porosity effect with PPI = 10 and horizontal (H) configuration

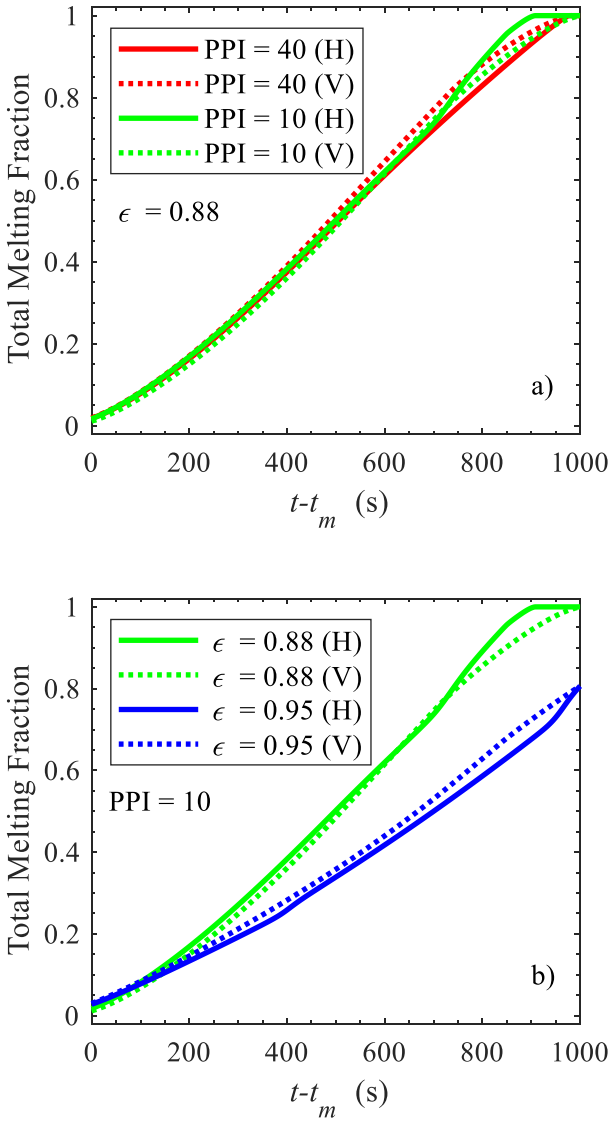

Fig. 21 – Total melting fractions evolution with time for horizontal (H) and vertical (V) configurations and foam morphological characteristics: a) PPI effect and b) porosity effect

5. Conclusions

In this paper, both experimental and numerical results on phase change material coupled with aluminum foams have been presented for different gravity orientation, heat fluxes, porosities and PPIs. Twelve experiments have been performed. Melting front position has been established with a IR camera by employing a MATLAB algorithm, with which is possible to establish its position through time depending on the temperature measured. The numerical model is set up with references to the volume-averaged form of porous media equations, under the assumption of Local Thermal Non-Equilibrium (LTNE) between the two phases and non-negligible convection for the PCM fluid phase. The main objectives of the present paper are to assess the accuracy of the numerical model in many conditions, the development of a rigorous technique to establish melting front depending on measured or predicted temperatures, and to analyze various effects like convection in terms of device orientation, morphological properties importance and so

on. A very good agreement between experiments and simulations has been found here for all the experiments that have been ran. It has been shown that liquid phase convection strongly affects melting front position. In particular, this will not be exactly perpendicular to the applied heat flux anymore. For the vertical orientation, this distortion is strongly affected by porosity and PPI too. Higher porosity makes melting front more curved because of the reduced overall thermal conductivity. On the other hand, with lower PPIs melting zone in the top becomes slightly higher because of the increase of natural convection motion. In the horizontal orientation, Rayleigh-Benard cell can arise especially for higher porosities.

After comparisons, an analysis of the effects of heat losses due to external convection, and of melting temperature range has been carried out. Heat losses can have relevant effects on melting front position, making it more distorted, especially near the boundaries where there is convective heat loss to the environment. Melting temperature range has a qualitative effect on melting front position because the zone in which one can find both phases becomes more extended.

Finally, experimental and numerical results for total melting front evolution vs time have been compared, showing a good agreement. Various effects have been analyzed too in in different conditions. It has been shown that lower porosity foams make melting time shorter, while PPIs does not have relevant effects on this. With references to the orientation, a very small contribution from this has been observed here.

Acknowledgments

This work was supported by Italian Government MIUR Grant No. PRIN-2017F7KZWS.

References

[1] Faraj, K., Khaled, M., Faraj, J., Hachem, F., & Castelain, C. (2020). Phase change material thermal energy storage systems for cooling applications in buildings: A review. *Renewable and Sustainable Energy Reviews*, *119*, 109579.

[2] Qureshi, Z. A., Ali, H. M., & Khushnood, S. (2018). Recent advances on thermal conductivity enhancement of phase change materials for energy storage system: a review. *International Journal of Heat and Mass Transfer*, *127*, 838-856.

[3] Chen, J., Yang, D., Jiang, J., Ma, A., & Song, D. (2014). Research progress of phase change materials (PCMs) embedded with metal foam (a review). *Procedia Materials Science*, *4*, 389-394.

[4] Wang, G., Wei, G., Xu, C., Ju, X., Yang, Y., & Du, X. (2019). Numerical simulation of effective thermal conductivity and pore-scale melting process of PCMs in foam metals. *Applied Thermal Engineering*, *147*, 464-472.

[5] Mesalhy, O., Lafdi, K., Elgafy, A., & Bowman, K. (2005). Numerical study for enhancing the thermal conductivity of phase change material (PCM) storage using high thermal conductivity porous matrix. *Energy Conversion and Management*, *46*(6), 847-867.

[6] Lafdi, K., Mesalhy, O., & Shaikh, S. (2007). Experimental study on the influence of foam porosity and pore size on the melting of phase change materials. *Journal of Applied Physics*, *102*(8), 083549.

[7] Zhao, C. Y., Lu, W., & Tian, Y. (2010). Heat transfer enhancement for thermal energy storage using metal foams embedded within phase change materials (PCMs). *Solar energy*, *84*(8), 1402-1412.

[8] Tian, Y., & Zhao, C. Y. (2011). A numerical investigation of heat transfer in phase change materials (PCMs) embedded in porous metals. *Energy*, *36*(9), 5539-5546.

[9] Li, W. Q., Qu, Z. G., He, Y. L., & Tao, W. Q. (2012). Experimental and numerical studies on melting phase change heat transfer in open-cell metallic foams filled with paraffin. *Applied Thermal Engineering*, *37*, 1-9.

[10] Xiao, X., Zhang, P., & Li, M. (2014). Effective thermal conductivity of open-cell metal foams impregnated with pure paraffin for latent heat storage. *International Journal of Thermal Sciences*, *81*, 94-105.

[11] Mancin, S., Diani, A., Doretti, L., Hooman, K., & Rossetto, L. (2015). Experimental analysis of phase change phenomenon of paraffin waxes embedded in copper foams. *International Journal of Thermal Sciences*, *90*, 79-89.
[12] Yang, X., Feng, S., Zhang, Q., Chai, Y., Jin, L., & Lu, T. J. (2017). The role of porous metal foam on the unidirectional solidification of saturating fluid for cold storage. *Applied energy*, *194*, 508-521.
[13] Li, W., Wan, H., Lou, H., Fu, Y., Qin, F., & He, G. (2017). Enhanced thermal management with microencapsulated phase change material particles infiltrated in cellular metal foam. *Energy*, *127*, 671-679.
[14] Di Giorgio, P., Iasiello, M., Viglione, A., Mameli, M., Filippeschi, S., Di Marco, P., ... & Bianco, N. (2017). Numerical analysis of a paraffin/metal foam Composite for Thermal Storage. In *Journal of Physics: Conference Series* (Vol. 796, No. 1, p. 012032). IOP Publishing.
[15] Diani, A., & Campanale, M. (2019). Transient melting of paraffin waxes embedded in aluminum foams: Experimental results and modeling. *International Journal of Thermal Sciences*, *144*, 119-128.
[16] Ferfera, R. S., Madani, B., & Serhane, R. (2020). Investigation of heat transfer improvement at idealized microcellular scale for metal foam incorporated with paraffin. *International Journal of Thermal Sciences*, *156*, 106444.
[17] Muhammad Mansoor Janjua, Uzair Sajjad, Wei-Mon Yan. A critical review on heat transfer augmentation of phase change materials embedded with porous materials/foams. International Journal of Heat and Mass Transfer, vol. 135, pp. 649-673 (2019).
[18] Zhang, S., Feng, D., Shi, L., Wang, L., Jin, Y., Tian, L., ... & Yan, Y. A review of phase change heat transfer in shape-stabilized phase change materials (ss-PCMs) based on porous supports for thermal energy storage. Renewable and Sustainable Energy Reviews, 135, 110127.
[19] Filippeschi S., Mameli M., Di Marco P., (2018) Experimental Analysis of the Melting Process in A Pcm/Aluminum Foam Composite Material in Hypergravity Conditions, Interfacial Phenomena and Heat Transfer, 6(4), 451–467 (2018).
[20] Hu, X., Zhu, F., & Gong, X. (2020). Numerical investigation of the effects of heating and contact conditions on the thermal charging performance of composite phase change material. *Journal of Energy Storage*, *30*, 101444.
[21] Zhang, P., Meng, Z. N., Zhu, H., Wang, Y. L., & Peng, S. P. (2017). Melting heat transfer characteristics of a composite phase change material fabricated by paraffin and metal foam. *Applied Energy*, *185*, 1971-1983.
[22] Chen, Z., Gao, D., & Shi, J. (2014). Experimental and numerical study on melting of phase change materials in metal foams at pore scale. *International journal of heat and mass transfer*, *72*, 646-655.
[23] Kaviany, M. (2012). *Principles of heat transfer in porous media*. Springer Science & Business Media.
[24] Amiri, A., & Vafai, K. (1994). Analysis of dispersion effects and non-thermal equilibrium, non-Darcian, variable porosity incompressible flow through porous media. *International journal of heat and mass transfer*, *37*(6), 939-954.
[25] Kheirabadi, A. C., & Groulx, D. (2015). The effect of the mushy-zone constant on simulated phase change heat transfer. In *Proceedings of CHT-15. 6 th International Symposium on ADVANCES IN COMPUTATIONAL HEAT TRANSFER*. Begel House Inc..
[26] Calmidi, V. *Transport phenomena in high porosity fibrous metal foams, 1998* (Doctoral dissertation, Ph. D thesis, University of Colorado).
[27] Andreozzi A., Bianco N., Iasiello M. & Naso V. (2019). Natural convection in a vertical channel with open-cell foams. Proceedings of the 37th UIT Conference, Padova (Italy), 24-26 June
[28] Churchill, S. W., & Chu, H. H. (1975). Correlating equations for laminar and turbulent free convection from a horizontal cylinder. *International journal of heat and mass transfer*, *18*(9), 1049-1053.
[29] Georgiadis, J. G., & Catton, I. (1988). Dispersion in cellular thermal convection in porous layers. *International journal of heat and mass transfer*, *31*(5), 1081-1091.
[30] Iasiello, M., Bianco, N., Chiu, W. K. S., & Naso, V. (2019). Thermal conduction in open-cell metal foams: Anisotropy and Representative Volume Element. *International Journal of Thermal Sciences*, *137*, 399-409.

[31] Hwang, G. J., Wu, C. C., & Chao, C. H. (1995). Investigation of non-Darcian forced convection in an asymmetrically heated sintered porous channel.
[32] Feng, S., Shi, M., Li, Y., & Lu, T. J. (2015). Pore-scale and volume-averaged numerical simulations of melting phase change heat transfer in finned metal foam. *International Journal of Heat and Mass Transfer, 90*, 838-847.

DESTEC
UNIVERSITÀ DI PISA

Dipartimento di Ingegneria dell'Energia, dei Sistemi, del Territorio e delle Costruzioni

Largo Lucio Lazzarino – 56122, Pisa (Italy)
Tel. +39 050 2217300, Fax + 39 050 2217333
Partita IVA 00286820501 VAT No. IT00286820501
Codice fiscale 80003670504

To,
Prof. Dr. C.N. Markides
Editor-in-Chief
Applied Thermal Engineering
Imperial College London, London, UK

Mauro Mameli
University of Pisa, DESTEC
Thermal Physics Laboratory
Tel: +39 050 2217166
E-mail: mauro.mameli@unipi.it

Date: September 4th, 2020

Dear Prof. Markides,

On behalf of all the authors of the manuscript entitled:

Experimental and numerical analysis of the melting evolution in phase change materials embedded with aluminum foams with different morphologies and orientations

Authors: Marcello Iasiello, Mauro Mameli, Sauro Filippeschi and Nicola Bianco

E-mail of the corresponding Author (Mauro Mameli): mauro.mameli@unipi.it

I hereby declare that:

- All authors have participated in conception and design, or analysis and interpretation of the data; drafting the article or revising it critically for important intellectual content; and approval of the final version.
- This manuscript has not been submitted to, nor is under review at, another journal or other publishing venue.
- The authors have no affiliation with any organization with a direct or indirect financial interest in the subject matter discussed in the manuscript.

Yours sincerely,

Mauro Mameli
(Corresponding Author)